HHS Public Access

Author manuscript

Cell Rep. Author manuscript; available in PMC 2017 July 26.

Published in final edited form as:

Cell Rep. 2017 June 06; 19(10): 2157–2173. doi:10.1016/j.celrep.2017.05.045.

Tcrd rearrangement redirects a processive *Tcra* recombination program to expand the *Tcra* repertoire

Zachary M. Carico[1], **Kingshuk Roy Choudhury**[2], **Baojun Zhang**[1], **Yuan Zhuang**[1], and **Michael S. Krangel**[1,3]

[1]Department of Immunology, Duke University Medical Center, Durham, North Carolina, USA

[2]Department of Biostatistics and Bioinformatics, Duke University Medical Center, Durham, North Carolina, 27710, USA

SUMMARY

Adaptive immunity depends on diverse T cell receptor repertoires generated by V(D)J recombination. Here, we define the principles by which combinatorial diversity is generated in the murine *Tcra* repertoire. *Tcra* and *Tcrd* gene segments share the *Tcra-Tcrd* locus, with interspersed V_α and V_δ segments undergoing V_δ-D_δ-J_δ rearrangement in $CD4^-CD8^-$ thymocytes and then multiple rounds of V_α–J_α rearrangement in $CD4^+CD8^+$ thymocytes. We document stepwise, highly coordinated proximal-to-distal progressions of V_α and V_δ use on individual *Tcra* alleles, limiting combinatorial diversity. This behavior is supported by an extended chromatin conformation in $CD4^+CD8^+$ thymocytes, with only nearby V_α and V_δ segments contacting each other. *Tcrd* rearrangements can use distal V_δ segments due to a contracted *Tcra-Tcrd* conformation in $CD4^-CD8^-$ thymocytes. These rearrangements expand the *Tcra* repertoire by truncating the V_α array to permit otherwise disfavored V_α–J_α combinations. Therefore, recombination events at two developmental stages with distinct chromatin conformations synergize to promote *Tcra* repertoire diversity.

ETOC BLURB

A diverse *Tcra* repertoire is essential for robust adaptive immunity. Carico et al. demonstrate that the *Tcra* repertoire is intrinsically limited by a processive recombination program. *Tcrd* recombination overcomes this constraint to broaden V_α-J_α combinatorial diversity, and is important for development of MAIT cells, an innate-like αβ T cell subset.

Correspondence: krang001@mc.duke.edu.
[3]Lead Contact

AUTHOR CONTRIBUTIONS

Z.C., K.R.C., B.Z., Y.Z. and M.S.K conceived and designed the experiments, Z.C. and B.Z. performed the experiments, Z.C., K.R.C. and M.S.K. analyzed the experiments, and Z.C., K.R.C. and M.S.K. wrote the manuscript.

ACCESSION NUMBERS

TCRα repertoire sequencing and 4C-seq data are deposited in the Gene Expression Omnibus (GSE95826).

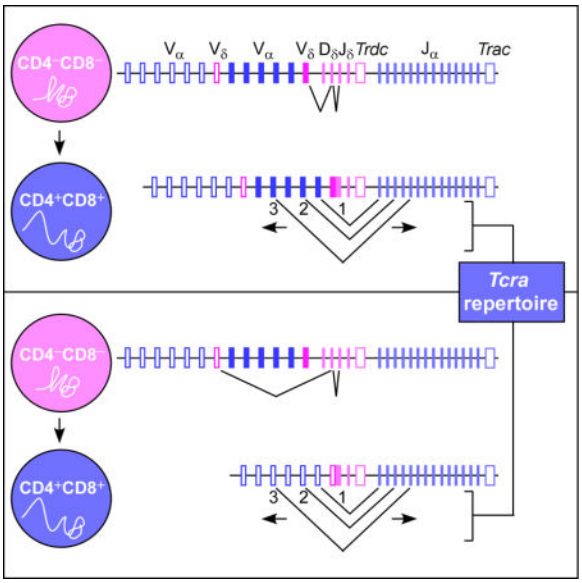

Keywords

antigen receptor; chromatin conformation; mucosa-associated invariant T cells; MAIT cells; T cell receptor alpha; T cell receptor delta; T cell development; TCR repertoire; T cell receptor repertoire; V(D)J recombination

INTRODUCTION

Vertebrate adaptive immune systems depend on V(D)J recombination to generate pools of diverse, clonally distributed antigen receptors (AgRs) on T and B lymphocytes. AgR loci contain arrays of variable (V), joining (J), and at some loci, diversity (D) gene segments, which are joined during lymphocyte development to create complete AgR genes. This process is catalyzed by the lymphoid-specific recombination-activating gene (RAG) protein complex, which generates site-specific DNA double-strand breaks between V, D, and J coding gene segments and their associated recombination signal sequences (RSSs) (Schatz and Swanson, 2011). RAG initially binds to discrete regions containing highly transcribed and accessible D and J gene segments under control of developmentally-regulated enhancer and promoter elements, forming a chromatin structure called the recombination center (RC) (Schatz and Ji, 2011). RC-bound RAG is then thought to capture distant V segment RSSs to mediate V-to-(D)J recombination and complete assembly of the AgR gene. AgR diversity is generated by combinatorial usage of V, D, and J segments, together with DNA repair mechanisms associated with non-homologous end joining, which impart heterogeneity to the junctions between coding gene segments (Helmink and Sleckman, 2012).

T lymphocyte development generates distinct lineages of T cells bearing either a γδ or an αβ T cell receptor (TCR). Notably, the gene segments encoding TCRδ and TCRα chains are arrayed in a single genetic locus, *Tcra-Tcrd*. In mice, D_δ, J_δ, and *Trdc* (C_δ) gene segments are nested between a 1.5 Mb array of more than 100 V_α and V_δ segments and a 60 kb region containing 60 J_α segments and *Trac* (C_α) (Carico and Krangel, 2015). There are nominally

16 V_δ gene segments interspersed across the V_α-V_δ array; whereas the pool of V_δ segments is limited, almost all V segments (V_α and V_δ) contribute to the *Tcra* repertoire. During the $CD4^-CD8^-$ double-negative (DN) stage of T cell development, *Tcrd* undergoes biallelic V_δ-D_δ-J_δ rearrangement. In parallel, DN thymocytes also rearrange *Tcrg* and *Tcrb;* expression of a γδ TCR commits cells to the γδ -lineage, while expression of a TCRβ protein commits cells to the αβ-lineage (Ciofani and Zúñiga-Pflücker, 2010). *Tcra* then undergoes biallelic V_α-J_δ rearrangement in the $CD4^+CD8^+$ (DP) compartment (Carico and Krangel, 2015). *Tcra* is striking for its tendency to undergo multiple rounds of V-J rearrangement on each allele, allowing multiple opportunities to create TCRαβ-bearing thymocytes that can undergo positive selection. *Tcrd* and *Tcra* rearrangements are directed, in part, by the developmentally-regulated enhancers E_δ, which creates D_δ and J_δ accessibility in DN thymocytes, and E_α, which creates accessibility of J_α and some V_α segments in DP thymocytes (Hao and Krangel, 2011; Hawwari and Krangel, 2005). The nested *Tcra-Tcrd* structure is well-conserved among mammals, but the implications of this organization are unclear (Carico and Krangel, 2015; Glusman et al., 2001).

Although numerous studies have examined combinatorial diversity in the *Tcra* repertoire, the extent of diversity and its mechanistic underpinnings are only partially understood. J_α gene segment usage, and the mechanisms that regulate that usage, are well-established. Primary rearrangements are directed to the most V_α-proximal J_α segments due to activation of the T early alpha promoter (TEA) and additional J_α promoters by E_α (Abarrategui and Krangel, 2006; Guo et al., 2002; Hawwari et al., 2005; Thompson et al., 1990; Villey et al., 1996). Secondary rearrangements tend to use the most V_α-proximal of the remaining J_α segments, due to transcription driven from the rearranged V_α-J_α cassette (Buch et al., 2002; Hawwari and Krangel, 2007; Huang and Kanagawa, 2001; Pasqual et al., 2002; Petrie et al., 1995). Comparatively less is known about patterns of V_α usage (Carico and Krangel, 2015). A variety of PCR-based studies have documented that J_α-proximal V_α segments tend to rearrange to proximal J_α segments, whereas J_α-distal V_α segments tend to rearrange to distal J_α segments (Aude-Garcia et al., 2001; Huang and Kanagawa, 2001; Pasqual et al., 2002). Such biases could reflect a regulated mechanism governing V_α usage, or alternatively, the consequence of stochastic V_α usage through multiple rounds of V_α-J_α rearrangement. In contrast, high-throughput sequencing (HTS) of the *Tcra* repertoire in naïve $CD8^+$ T cells found that V_α-J_α combinations occurred mostly independent of chromosomal position (Genolet et al., 2012). This was interpreted to indicate that selection of V_α segments for rearrangement was primarily a stochastic process, with all V_α segments simultaneously available for recombination (Genolet et al., 2012). The discrepancies among these studies notwithstanding, given the highly regulated progression of J_α usage through multiple rounds of rearrangement, the manner in which V_α segments are used should have enormous implications for combinatorial diversity in the *Tcra* repertoire.

Here, we developed and applied a high-throughput sequencing (HTS)-based strategy to analyze the pre-selection *Tcra* repertoire in mice carrying wild-type and genetically modified *Tcra-Tcrd* alleles. We found that *Tcra* rearrangement in individual thymocytes is intrinsically highly processive and coordinated along the V_α and J_α arrays through multiple rounds of rearrangement, imposing severe constraints on combinatorial diversity. Repertoire diversity is nonetheless achieved by mechanisms that impart combinatorial diversity to

primary V_α-J_α rearrangement, effectively scrambling the starting points for progressions of secondary rearrangements in individual DP thymocytes. A major mechanism by which V diversity is imparted during primary V_α-J_α rearrangements is prior *Tcrd* recombination in DN thymocytes, which variably truncates the V_α array and allows distal V_α segments to rearrange to proximal J_α segments. Such diversification is functionally significant, as *Trav1-Traj33*$^+$ mucosa-associated invariant T (MAIT) cells are depleted when *Tcrd* rearrangement is impaired or absent.

RESULTS

Pre-selection *Tcra* repertoire in DP thymocytes

We developed an HTS approach to study the *Tcra* repertoire that was tailored to the specific challenges presented by the *Tcra-Tcrd* locus. Rather than amplifying gene segment joins directly from genomic DNA using multiplexed primers that target the many individual V and J segments, we analyzed rearrangements in *Tcra* transcripts using a single primer pair targeting C_α and a common adapter added to the 5′ ends of cDNA during 5′ rapid amplification of cDNA ends (5′ RACE). To unambiguously differentiate between the many highly similar V_α gene segment family members, we obtained long sequencing reads through the V_α-J_α coding region using 300-nucleotide paired-end sequencing on the Illumina MiSeq platform. We used the powerful MiXCR immune repertoire analysis software, which aided with sequence calls and allowed us to count V_α-J_α joins from unique clones only (Bolotin et al., 2015). We also used strain 129 mice, because the 129 *Tcra* haplotype contains a less complex V_α array including a 400kb duplication, rather than a triplication as in C57BL/6 (Carico and Krangel, 2015). Our approach allowed for accurate identification of all V_α segments by software except for *Trav16* and *Trav16d*, which we were able to unambiguously distinguish through manual analysis. We were unable to measure primary rearrangements involving pseudogene *Traj61*, because it lacks functional splice signals and would not be captured by 5′ RACE (Villey et al., 1997).

We measured V_α and J_α usage in wild-type $CD4^+CD8^+CD3\varepsilon^{lo}$ thymocytes to assess the pre-selection *Tcra* repertoire (Table S1). We detected a clear bias for usage of proximal V_α with proximal J_α and distal V_α with distal J_α (Figure 1). Nonetheless, we were struck by the extent of combinatorial diversity, particularly in primary V_α-J_α recombination. We defined the V segments used in primary rearrangement as those joined to the most proximal J_α segment analyzed, *Traj58.* Similarly, we defined the J_α segments used in primary rearrangement as those joined to the most proximal V_α segment used, *Trdv2-2. Traj58* most frequently rearranged to very proximal V_α segments *Trdv2-2, Trdvl, Trav21*, and *Trav19* (Figures 1B and 1C). However, *Traj58* also rearranged extensively to V_α segments distributed across 750 kb, including a large portion of the central V_α array. Moreover, some *Traj58* rearrangements involved a cluster of V_α segments located in the central duplication region (Figures 1B and 1C). Similarly, *Trdv2-2* rearranged to J_α segments as distal as *Traj26* (Figures 1B and 1C). We noted at least two apparent ‘tracks’ along which subsequent (secondary) V_α-J_α rearrangements occurred: a major diagonal initiating from primary rearrangements involving *Trdv2-2* to *Trav6-6* and *Traj58* to *Traj26*, and a minor ‘shadow’

diagonal arising from primary J_α rearrangements to distal V_α segments in the central-duplication region.

Developmental progression of V_α-J_α rearrangement

To better understand the inferred progression of V_α-J_α rearrangements through primary and multiple rounds of secondary recombination, we examined the distribution of rearrangements in a fixed cohort of DP thymocytes over time. To do this, we injected mice bearing *Tcrd*$^{\text{CreER}}$ and *Rosa26*$^{\textit{fl-STOP-fl-ZsGreen}}$ alleles (Zhang et al., 2015) with tamoxifen to label DN thymocytes, which express *Tcrd*, and we tracked *Tcra* rearrangements in those cells over time as they entered into and matured in the DP compartment. A single dose of tamoxifen preferentially labeled DN2 and DN4-CD8 ISP thymocytes, which progressively moved into the DN3 and DP compartments, respectively, over 72 hrs (Figure S1A). As expected, ZsGreen$^+$ DP thymocytes were CD71$^+$ at early times but were largely CD71$^-$ by 48 hrs. ZsGreen$^-$ DP thymocytes were always CD71$^-$, indicating that they represented older DP thymocytes at all time points (Figure S1B).

Twelve hours after tamoxifen injection, ZsGreen$^+$CD4$^+$CD8$^+$CD3ε^{lo} thymocytes displayed Jα usage heavily biased toward proximal segments between *Traj58* and *Traj26*, and usage became progressively more distal at 24−, 48−, and 72 hrs (Figures 2A and 2B). V_α usage similarly progressed from proximal to distal in the same time frame. At all times examined, ZsGreen$^-$CD4$^+$CD8$^+$CD3ε^{lo} thymocytes displayed usage of more distal V_α-J_α segments than their ZsGreen$^+$ counterparts, consistent with ZsGreen$^-$ cells representing an older cohort of DP thymocytes.

The time course experiment also emphasized the tremendous heterogeneity of the earliest *Tcra* rearrangement events (Figures 2A, 2B, and S1C). Va usage was broadly distributed across the proximal half of the Vα array and included a cluster in the central duplication region that was even more striking than in steady-state conditions (Figures 1B and 1C). Notably, usage of the central duplication V_α cluster was mirrored by prominent usage of the homologous cluster of V_α segments in the central V_α region at 12 hrs post-injection (Figures 2B and S1C). Moreover, from all points in the 12-hr V_α-J_α distribution, rearrangements progressed to correspondingly more distal V_α-J_α combinations over time.

V_α-J_α rearrangements are highly processive in individual DP thymocytes

To better understand the dynamics of V_α-J_α rearrangement, we analyzed the distribution of secondary rearrangements in DP thymocytes of mice in which all thymocytes bear a uniform primary V_α-J_α rearrangement (Figure 3A). HYα mice carry a *Trav17-Traj57* rearrangement introduced into *Tcra* with deletion of 280kb from *Trav21* to *Traj57* (Buch et al., 2002). In the absence of the HY-specific TCRβ chain, most DP thymocytes fail to undergo positive selection due to HYα, and undergo multiple rounds of secondary V_α-J_α recombination, deleting the initial *Trav17-Traj57* rearrangement (Buch et al., 2002; Hawwari and Krangel, 2007). We found that combinatorial diversity was greatly constrained downstream of the fixed primary rearrangement in pre-selection thymocytes, with strong enrichment for “on-diagonal” V_α-J_α combinations and suppressed usage of distal V_α with proximal J_α segments (Figure 3B, 3C and S2A). Moreover, the repertoire observed in pre-selection DP thymocytes

was not substantially modified by selection, because resting $CD8^+CD44^-CD62L^+$ splenic T cells displayed a similarly constrained distribution of V_α-J_α combinations (Figure S2B).

To better understand how V_α usage changes as rearrangement proceeds, we plotted the frequency-weighted means and standard deviations (SD) of the chromosomal coordinates of the V_α segments used with each J_α segment in HYα DP thymocytes (Figures 4A and 4B). We observed that both values increased in approximately linear fashion across a substantial portion of the J_α array, but leveled off in the distal J_α segments. We calculated that in the linear region, the mean increased at a rate of 12.76 bp of V_α DNA for every one bp of J_α DNA (Table S2). Since V_α segments are, on average, spaced at 9.6 times the distance between J_α segments, this corresponds to movement of 1.33 V per J throughout the bulk of the V_α and J_α arrays. The SD increased from a starting value of 107,898 bp at *Traj56* at a rate of 3.89 bp of V_α DNA for every one bp of J_α DNA (Table S2). Deviation from these trends across the distal Jα segments reflects the constraints imposed on V_α usage as the V_α array is exhausted.

The above analysis suggested that rearrangements in individual thymocytes are highly processive along the V_α and J_α arrays, with movement described by a linear drift model, in which a constant rate of progression of V_α position is subject to random error that accumulates as the process iterates. To test this model, we simulated V_α-J_α rearrangement in 1000 individual cells using the observed starting values at *Traj56* and the slopes for the mean and SD progressions. The linear drift simulation explained the observed mean and standard deviation plots remarkably well, irrespective of whether successive J_α rearrangements were assumed to occur in steps of one, five or ten J_α segments (Figures 4A and 4B). We also simulated V_α segment selection as a random choice, which assumed a uniform probability for all remaining V_α segments at each step in the rearrangement process. Regardless of the J_α step function tested, these models poorly described the observed data (Figures 4A and 4B), because they too rapidly consumed the V_α array. This analysis highlighted that usage of the V_α and J_α arrays in individual thymocytes is both highly processive and highly coordinated throughout many rounds of secondary rearrangement, placing substantial constraints on combinatorial diversity.

Tcra combinatorial diversity depends upon truncation of V_α array by *Tcrd* rearrangement

Because of the highly processive nature of secondary rearrangements in individual thymocytes, diversity in the pre-selection *Tcra* repertoire is heavily dependent on primary *Tcra* rearrangement. In wild-type mice, DP thymocytes initiating *Tcra* rearrangement have previously undergone V_δ-to-D_δ rearrangement on about 70% of *Tcra-Tcrd* alleles (Livak et al., 1995; Nakajima et al., 1995; Shih et al., 2012). Because V_δ segments are dispersed across one Mb within the Va array (Figure 5A), V_δ-to-D_δ recombination would variably truncate the Vα array and alter the starting point for primary V_α-to-J_α rearrangement in individual DP thymocytes. Consistent with that idea, we noted that the central and central-duplication V_α gene repeats used in primary V_α-J_α recombination tended to be located just distal to four members of the *Trav15-dv6* family (Figure 1A, red dots; Figure S1C), which are frequently used during *Tcrd* rearrangement (Weber-Arden et al., 2000; Zhao et al., 2016).

To better understand the role of *Tcrd* rearrangement in diversifying primary V_α-to-J_α rearrangements, we examined the *Tcra* repertoire in INT1-2-deficient mice (Chen et al., 2015). In these mice, deletion of two CTCF sites disrupts a chromatin structural loop that contains the *Tcrd* RC. Absence of the loop causes increased contacts between the *Tcrd* RC and proximal V_δ segments, increased RAG tracking from the RC to proximal V_δ segments, and, as a consequence, substantially increased rearrangement of proximal V_δ segments *Trdv2-2* and *Trdv3* at the expense of more distal V_δ segments, including the *Trav15-Trdv6* family (Chen et al., 2015; Zhao et al., 2016). Analysis of the pre-selection *Tcra* repertoire in INT1-2-deficient thymocytes revealed highly constrained global V_α-J_α combinatorial diversity, with a marked reduction in primary rearrangements using V_α segments in the central and central-duplication portions of the V_α array, and secondary rearrangements strongly biased toward “on-diagonal” combinations (Figures 5B and 5C). In fact, the V_α distribution used in early J_α rearrangements, as well as the overall distribution of V_α usage, mimicked the respective profiles in HYα thymocytes, even though patterns of J_α usage mirrored those in WT thymocytes (Figures S3A and S3B). Notably, INT1-2-deficient and HYα thymocytes both displayed reduced usage of distal V_α segments (Figures S3A and S3B), indicating failure to efficiently utilize the full length of the V_α array.

Quantitative analysis revealed that average V_α usage as a function of J_α position in INT1-2-deficient thymocytes was indistinguishable from HYα thymocytes, whereas both were clearly different from wild-type (Figure S4A and Table S2). However, the SD for initial V_α usage in INT1-2-deficient thymocytes was intermediate between that of wild-type and HYα (Figure S4B and Table S2). Nevertheless, in the region spanning *Traj52-Traj37*, the rates of $V_\alpha$movement and accumulation of V_α error were statistically indistinguishable for the three genotypes (Table S2). We conclude that limiting or eliminating *Tcrd* rearrangement has a major impact on the distribution of V_α gene segments used in primary rearrangements. However, because the means and SDs of V_α usage each changed at highly similar rates, we conclude that the mechanism of processive secondary rearrangements is common to all genotypes.

Tcra chromatin structure supports processive usage of V_α segments during *Tcra* rearrangement

Our previous studies by three-dimensional DNA fluorescence *in situ* hybridization (3D DNA FISH) showed that the unrearranged *Tcra-Tcrd* locus is highly contracted in DN thymocytes, but in DP thymocytes adopts a configuration in which the majority of V gene segments extend away from a compact region containing the *Tcra* and *Tcrd* RCs (Shih and Krangel, 2010). Studies using chromatin conformation capture (3C) revealed extensive contacts between proximal V_α and proximal J_α segments within the compact portion of the locus in DP thymocytes (Shih et al3., 2012). This genomic architecture can be understood to support proximally biased primary V_α-J_α rearrangement, with secondary rearrangements proceeding in highly processive fashion. To investigate the structure of unrearranged *Tcra-Tcrd* alleles in greater detail, we obtained DP thymocytes from *Rag2*$^{-/-}$ mice that had been injected with anti-CD3ε antibody, and performed 4C-seq from four viewpoints spanning from *Trav1* to E_α. In accord with prior studies, we observed an extensive network of interactions involving proximal V_α gene segments, the TEA promoter, and E_α (Figure 6A, top). However, distal

V_α segment *Trav1* and central duplication V_α segment *Trav14d-3* interacted neither with each other nor with the *Tcra* RC, implying an extended configuration for those portions of the locus.

The above analysis provided information relevant to the structure of the unrearranged locus, but whether this structure is maintained by a V_α-J_α rearranged locus, the substrate for secondary recombination, was unknown. Consequently, we analyzed interactions from several of the same viewpoints in DP thymocytes obtained from anti-CD3ε-treated HYα × *Rag2*$^{-/-}$~ mice. Because the TEA promoter is included in the 280kb deletion on the HYα allele, we analyzed interactions using the *Trav17-Traj57* cassette as a viewpoint instead. Despite the large deletion, E_α and *Trav17-Traj57* contacted neither distal nor central duplication V_α segments, and *Trav1* and *Trav14d-3* contacted neither the *Tcra* RC nor each other (Figure 6A, bottom). Nevertheless, as a consequence of the deletion, viewpoints in the *Tcra* RC interacted more frequently with proximal and some central V_α segments (Figure 6A, bottom), a point which was confirmed by 3C (Figure 6B). Because contacts with the RC were redirected to the most proximal of the remaining V_α segments on the HYα allele, these contact profiles suggest a straightforward structural explanation for processive use of V_α gene segments during secondary recombination.

As additional evidence that many V segments remain out of contact with the *Tcra* RC on rearranged alleles, we compared HYα to wild-type alleles by 3D DNA-FISH. To accomplish this, we generated DP thymocytes from *Rag2*$^{-/-}$ mice heterozygous for the HYα allele, and used a three-probe strategy in which two probes (A and B) measured the distance between distal and central V_α gene segments, and one probe (C) distinguished the wild-type allele (intense hybridization) from the HYα allele (minimal hybridization). We observed virtually indistinguishable distributions of V_α configurations on WT and HYα alleles, confirming that the V_α array remains relatively extended through primary and secondary recombination (Figure S5).

MAIT cell development depends on diversification of *Tcra* repertoire by *Tcrd* rearrangement

A striking feature of the repertoires of HYα and INT1-2-deficient mice is the loss of rearrangements of central J_α segments to distal V_α segments (Figures 3B and 5B). Among the affected V_α-J_α combinations is *Trav1-Traj33*, which is less frequent in both HYα and INT1-2-deficient thymocytes relative to wild-type (Figure 7A). This rearrangement is notable because it encodes the invariant TCRa chain used by mucosa-associated invariant T (MAIT) cells (Godfrey et al., 2015; Tilloy et al., 1999). MAIT cells represent an innate-like T cell lineage that is selected by and responds to bacterial vitamin B metabolites presented by MHC-related protein 1 (MR1)(Godfrey et al., 2015). At mucosal surfaces, MAIT cells play a vital role in the response to a variety of bacterial pathogens (Le Bourhis et al., 2010; Meierovics et al., 2013). To determine whether MAIT cell abundance is reduced as a consequence of diminished *Tcrd* rearrangement, we used fluorophore-conjugated, antigen-loaded MR1 tetramers (Corbett et al., 2014) to compare MAIT cell populations by flow cytometry in peripheral immune tissues of wild-type, HYα, and INT1-2-deficient mice (Figures 7B and 7C). We detected 52% and 57% reductions in MR1-tetramer$^+$ cell

frequencies in spleens and lungs of INT1-2-deficient mice, and 77% and 76% reductions in spleens and lungs of HYα mice, respectively, relative to wild-type (Figures 7B and 7C). We conclude that the frequency of *Trav1-Traj33* rearrangements in the thymus informs MAIT cell numbers in the periphery and that a replete MAIT cell compartment is a major functional consequence of *Tcrd* rearrangement on αβ-lineage T cells.

DISCUSSION

Here, we have defined the principles by which combinatorial diversity is generated in the pre-selection *Tcra* repertoire. Our analysis of the steady state distribution of rearrangements in wild-type and genetically manipulated strains of mice, and the temporal progression of rearrangements in wild-type mice, revealed regulated usage of both V_α and J_α segments. Primary V_α-J_α recombination events were remarkably diverse, engaging nearly half of all V_α and J_α segments. However, once a specific V_α-J_α combination was chosen during primary rearrangement in a young DP thymocyte, the subsequent progression of secondary rearrangements was highly processive, substantially constraining the set of V_α-J_α combinations available to that DP thymocyte. Notably, a major influence on the diversification of V_α usage during primary rearrangement was variable truncation of the V_α array by V_δ-D_δ rearrangements in DN thymocytes. This not only scrambled the starting points for primary rearrangement in thymocytes entering the DP compartment, but also made available distinct sets of V_α-J_α combinations during subsequent rounds of V-to-J rearrangement. Thus, heterogeneous *Tcrd* rearrangements in DN thymocytes enhance combinatorial diversity in the *Tcra* repertoire by mitigating the constraints imposed by processive usage of V_α and J_α segments during secondary rearrangements.

Primary rearrangements are also made diverse by mechanisms that promote the usage of a substantial portion of the J_α array. Although it is understood that primary rearrangements are biased towards use of J_α segments at the V_α-proximal end of the J_α array, our results revealed an unexpectedly broad distribution of primary rearrangements from *Traj58* to *Traj26.* This distribution stands in striking contrast to the set of J_α segments used during the initial cycle of secondary recombination on HYα alleles, which we show involves only a few of the most V_α-proximal J_α segments. This difference in J_α usage during primary and secondary recombination is consistent with previously established distributions of RAG proteins on the unrearranged wildtype and the HYα allele (Ji et al., 2010a, 2010b), and can be understood as a consequence of differentially-regulated promoter usage. Unrearranged alleles are characterized by E_α-dependent germline transcription originating from the TEA promoter and a series of weaker J_α promoters dispersed through the V_α-proximal one-third of the J_α array (Abarrategui and Krangel, 2006; Hawwari et al., 2005; Villey et al., 1997). Transcription from these promoters creates the chromatin accessibility required for RAG binding. After primary rearrangement, transcription from the rearranged Vα promoter effectively suppresses transcription from downstream Jα promoters, thereby restricting RAG binding to the J_α segments immediately downstream (Hawwari and Krangel, 2007; Ji et al., 2010a). This more restricted targeting of J_α segments is likely to translate to their processive usage during secondary rearrangements.

Our results indicate that during primary and secondary rearrangement, V_α usage is restricted to the most proximal of the available V_α segments. We believe that this intrinsic bias to proximal V_α usage is best explained by the unique conformation of the *Tcra-Tcrd* locus in DP thymocytes. As demonstrated in this and previous studies, E_α, the *Tcra* RC, and proximal V_α gene segments contact each other within a relatively compact portion of the locus on unrearranged wild-type alleles, whereas more distal V_α gene segments reside in an extended region that does not contact the *Tcra* RC (Shih and Krangel, 2010; Shih et al., 2012). Because this structure is also maintained on the HYα allele following primary rearrangement, we imagine that only the most proximal V_α segments on an allele are likely to be captured by J_α-bound RAG, thus enforcing processive Va usage. That said, highly processive usage of V_α segments may also be understood as a consequence of RAG tracking. Recent studies have argued that RAG bound to an RSS in the RC can track along chromatin to find an RSS partner (Hu et al., 2015). Such a mechanism would impose a natural bias towards usage of relatively proximal V_α gene segments, thus enforcing processivity. Our data do not allow us to distinguish these two very different mechanisms for processive V_α usage.

As noted above, the extended conformation of the *Tcra-Tcrd* locus in DP thymocytes limits combinatorial diversity during any particular round of secondary rearrangement. Therefore, V-to-J rearrangement is required, not only to create TCRs to be tested by positive selection, but also to modify the locus by DNA deletion to create new opportunities for combinatorial diversity in subsequent rounds of rearrangement. At the same time, our results argue that *Tcra* combinatorial diversity is significantly enhanced by the quite distinct, fully contracted conformation of the locus in DN thymocytes (Shih and Krangel, 2010). As is the case at other antigen receptor loci, this contracted conformation is thought to allow distal and proximal V gene segments to effectively compete with each other for access to the RC (Jhunjhunwala et al., 2009; Shih and Krangel, 2013). In this regard, we presume that *Tcra-Tcrd* locus contraction in DN thymocytes is essential for members of the distributed *Trav15-dv6* family to make meaningful contributions to the *Tcrd* repertoire (Shih and Krangel, 2010). Since these and other *Tcrd* rearrangements then contribute to the heterogeneity of primary *Tcra* rearrangements in DP thymocytes, the *Tcra* repertoire appears to be shaped by the combined influences of two very different locus conformations in DN and DP thymocytes.

Our conclusions about the nature of the *Tcra* repertoire in wild-type mice stand in contrast with another study, which concluded that secondary V_α-J_α rearrangements occurred independent of V_α chromosomal positions (Genolet et al., 2012). We note, however, that this study analyzed C57BL/6 mice, which have a large triplication rather than duplication in the V_α array, and as a result, larger families of highly similar V_α-V_α segments. Moreover, their HTS approach, with only 100-nucleotide paired-end reads, allowed unambiguous assignment of only 60% of V_α sequence reads. Nevertheless, the remaining 40% of V_α sequence reads were assigned by distributing them among the relevant V_α family members. We believe that this approach would obscure the dynamics that were readily apparent in our analysis of the strain 129 pre-selection DP thymocyte repertoire. We do not believe the different results can be attributed to analysis of splenic CD8 T cells in the previous study, because our analysis revealed that repertoire biases established in pre-selection DP

thymocytes were largely maintained in the periphery. Despite the differences noted above, the profile of primary rearrangements described herein appears similar to that reported previously (Genolet et al., 2012).

Finally, our study reveals functional consequences of *Tcrd* rearrangement on *Tcra* repertoire diversification. The *Trav1-Traj33* combination that encodes the invariant MAIT cell TCRα chain cannot be readily accessed by secondary rearrangements in DP thymocytes that join a proximal V_α to a proximal J_α during primary rearrangement. Our results indicate that *Trav1-Traj33* rearrangements are much more frequent in the DP progeny of DN thymocytes that had undergone V_δ-D_δ rearrangement involving distal V_δ gene segments *Trav15d-1-dv6d-1* or *Trav15d-2-dv6d-2.* Consistent with this, prior work mapped substantial strain variation in MAIT cell numbers to the *Tcra* locus itself (Cui et al., 2015).

From an evolutionary perspective, the combination of a nested *Tcra-Tcrd* organization and distal V_δ rearrangements may impart combinatorial advantage in species with an expanded V_α array. In this regard, like the mouse, the human *Tcra-Tcrd* locus has a prominent V_δ segment, *TRDV1*, situated in the middle of the V_α-V_δ array, relatively far from the *Tcrd* RC. Notably, the nested *Tcra-Tcrd* organization found in mammals is not found in frogs (Glusman et al., 2001; Parra et al., 2010), which nevertheless have extended arrays of V_α and J_α segments.

Assuming a similarly processive scheme of gene segment usage, we suggest that the combinatorial *Tcra* repertoire in the frog will fall short of that achieved in mice and humans.

EXPERIMENTAL PROCEDURES

Mice

Wild-type and $Rag2^{-/-}$ mice (Shinkai, 1992) were strain 129. $Tcrd^{CreER} \times Rosa26^{fl\text{-}STOP\text{-}fl\text{-}zsGreen}$ *mice* (Zhang et al., 2015), mice homozygous for the HYα allele (Buch et al., 2002; Hawwari and Krangel, 2007), and mice homozygous for the INT1-2 deletion (Chen et al., 2015), were all of a mixed 129 and C57/BL6 genetic origin, and were previously described. HYα mice were bred with $Rag2^{-/-}$ mice to generate $Rag2^{-/-}$ mice either homozygous or heterozygous for the HYα allele (Shinkai, 1992). Regardless of genetic background, all mice analyzed carried wild-type or mutant strain 129 *Tcra-Tcrd* alleles. Mice were housed in a specific-pathogen-free facility managed by the Duke University Division of Laboratory Animal Resources. Mice of both genders were included in all experiments; no differences on the basis of gender were noted. All mice were handled in accordance with protocols approved by the Duke University Institutional Animal Care and Use Committee.

Cell collection

Thymi and spleens were generally collected from mice at 4 weeks of age. To label developing thymocytes, $Tcrd^{CreER}$ 0D7 $Rosa26^{fl\text{-}STOP\text{-}fl\text{-}ZsGreen}$ mice were injected i.p. with a single dose of 1 mg tamoxifen (Sigma-Aldrich) in corn oil (Sigma-Aldrich), 12–72 hrs prior to sacrifice. To isolate DP thymocytes from $Rag2^{-/-}$ mice, mice were injected i.p. with 150 μg of anti-CD3ε antibody (2C11; Biolegend) in saline at 3 weeks of age, and thymi

were harvested 10 d later. For analysis of MAIT cells, spleens and lungs were collected from 8–10 week old mice. Single-cell suspensions from lung were prepared as described (Yu et al., 2016), with modifications. Briefly, mice were euthanized via CO_2 asphyxiation and perfused with 25 ml phosphate-buffered saline (PBS) through the right atrium to flush erythrocytes and non-adherent leukocytes from the pulmonary vasculature. Lungs were then inflated with 1× Hank's buffered saline solution (HBSS) containing 5% (vol/vol) fetal bovine serum (FBS), 1.5 mg/ml collagenase A (Sigma-Aldrich) and 0.4 mg/ml DNAse I (Sigma-Aldrich), and incubated in the same solution for 45 minutes at 37°C. The resulting mixture was vortexed to homogenize the digested tissue, and filtered through an 80 μm nylon mesh. The homogenate was then pelleted and incubated for one min in 150 mM NH_4Cl, 10mM $KHCO_3$, 0.1 mM EDTA, pH 7.4, to lyse erythrocytes. The reaction was quenched by addition of RPMI 1640 containing 10% (vol/vol) FBS, pelleted by centrifugation, and resuspended in the same buffer.

Flow cytometry and cell sorting

All antibodies were purchased from Biolegend, unless stated otherwise. Pre-selection DP thymocytes were identified by staining with antibodies to CD4 (GK1.5), CD8α (53–6.7), CD3e (2C11), and lineage (Lin) markers B220 (RA3-6B2), CD11b (M1/70), CD11c (p150/90; eBioscience), F4/80 (BM8), Gr-1 (RB6-8C5), and Ter-119 (TER-119). Pre-selection DP thymocytes were defined as $CD4^+CD8^+Lin^-CD3e^{lo}$ during sorting. Analysis of thymocytes in *Tcrd*^{CreER} *Rosa26*$^{fl\_STOP\_fl\_ZsGreen}$ mice included, in addition, antibodies to CD44 (IM7), CD25 (PC61), CD71 (RI7217), and CD69 (H1.2F3). Pre-immune $CD8^+$ splenocytes were isolated by staining with antibodies to CD4, CD8α, CD44, CD62L (MEL-14), CD3ε, and lineage markers, and were defined as $CD3\varepsilon^{hi}CD4^-CD8\alpha^+CD44^-CD62L^+Un^-$. To identify MAIT cells, single cell suspensions from lung and spleen were stained with antibodies and MR1-tetramers as described (Corbett et al., 2014). Briefly, lung and splenocytes were stained for 30 min at 23°C with antibodies to CD4, CD8α, CD44, TCRβ (H57–597), CD62L, lineage markers, and phycoerythrin-conjugated MR1-tetramers (NIH Tetramer Core Facility) loaded with either 5-(2-oxopropylideneamino)-6-D-ribitylaminouracil (5-OP-RU) or acetyl-6-formylpterin (Ac-6-FP) in PBS containing 2% (vol/vol) FBS. MAIT cells were defined as $Lin^-TCR\beta^+CD44^+CD62L^-$ and 5-OP-RU MR1 tetramer$^+$. Data were acquired on a BD FacsCanto II flow cytometer in 8-color configuration and cell sorting was conducted using a Beckman Coulter Astrios or MoFlo.

Preparation of *Tcra* repertoire sequencing libraries

10^6 sorted pre-selection DP thymocytes were lysed in Trizol (ThermoFisher) per manufacturer's specifications and either stored at −80°C or used immediately for RNA extraction. Total RNA was subjected to template-switch 5′ RACE as previously described (Pinto and Lindblad, 2010; Quigley et al., 2011), with modifications. Briefly, a mixture 10^6 cell equivalents of RNA, 1 μM 5′ RACE adapter sequence (5′-GTCGCACGGTCCATCGCAGCAGTCACArGrGrG-3′) and 1 μM oligo(dT)20 primer in 12 μl nuclease-free water was heated to 70°C for one min to disrupt RNA secondary structure and then lowered to −20°C for one min to snap-anneal the oligo$(dT)_{20}$ primer. The reaction was then adjusted to 250 mM Tris-HCl, pH 8.3, 375 mM KCl, 15 mM $MgCl_2$, 0.5

mM dNTPs and 5 mM dithiothreitol, before addition of 200 U Superscript II (ThermoFisher) in a final volume of 20 µl. The reaction was incubated for 2 hrs at 42°C to synthesize cDNA and add RACE adapter by template switching. Reverse transcriptase was then inactivated by incubation for 7 min at 72°C.

PCR amplification of 5′ RACE cDNA was performed as described (Quigley et al., 2011), with modifications. All PCRs used Kapa HiFi polymerase in 1× Kapa HiFi buffer (Kapa Biosystems) in 50 µl total volume. PCR reactions contained 0.375 µM antisense *Trac* primer (5′-TACACAGCAGGTTCTGGGTTCTGGATGT-3′), 0.02 µM sense RACE adapter primer 1 (5′-ACGCTGACGCTGAGCCTACCTGACGTCGCACGGTCCATCGCAGCAGTC-3′), and 0.4 µM sense RACE adapter primer 2 (5′-ACGCTGACGCTGAGCCTACCTGAC-3′). Touchdown PCR was performed using one cycle of 30 s at 98°C, five cycles of 10 s at 98°C and 2 min at 72°C, five cycles of 10 s at 98°C and 2 min at 70°C, ten cycles of 10 s at 98°C, 30 s at 65°C, and 2 min at 72°C, and 1 cycle of 10 min at 72°C. PCR products were then purified using a PCR purification kit (Qiagen) and U-Prep spin columns (Genesee) following manufacturer's specifications. Barcodes and Illumina adapter sequences were then added by PCR amplification as described, with modifications (Kozich et al., 2013). Sense primer, consisted of, from 5′ to 3′,Illumina P5 adapter sequence (5′-AATGATACGGCGACCACCGAGATCTACAC-3′), one of seven Nextera XT (Illumina) 8bp barcode sequences (N50x), a pad sequence (5′-TGTCGTCCTT-3′), and the RACE adapter primer 2 sequence. Antisense primer, consisted of, from 5′ to 3′, the Illumina P7 adapter sequence (5′-CAAGCAGAAGACGGCATACGAGAT-3′), the Nextera ×T N701 barcode (5′-TCGCCTTA-3′), a pad sequence (5′-AGTCAATCAA-3′), and the *Trac* antisense primer sequence. Both were used at 0.375 00BCM. For PCR2, PCR1 products were subjected to one cycle of 30 s at 98°C, 10 cycles of 10 s at 98°C, 30 sec at 65°C, and 2 min at 72°C, and one cycle of 10 min at 72°C. For both rounds of PCR, eight individual PCRs were run for each sample, after which products were pooled. After the second round of PCR, products were purified as described above and amplification of libraries was verified by gel electrophoresis. PCR yields were quantified using PicoGreen (ThermoFisher). All primers and oligonucleotides were obtained from Integrated DNA Technologies, purified using standard desalting methods, and dissolved in nuclease-free water.

Immune repertoire sequencing and data analysis

Either six or seven barcoded libraries were pooled in equimolar amounts for sequencing, which was performed by the Duke University Sequencing and Genomic Technologies Shared Resource using the Illumina MiSeq platform. Agilent Bioanalyzer traces were used to determine library molarity and quality prior to loading of the flow cell. Custom primers for sequencing read 1 (5′-GGTCCATCGCAGCAGTCACAGGGG-3′), the P7 index read (5′-CAGAACCCAGAACCTGCTGTGTATTGATTGACT-3′), and sequencing read 2 (5′-AGTCAATCAATACACAGCAGGTTCTGGGTTCTGGATGT-3′) were spiked into the standard Illumina primer mix along with a PhiX control library. 300 nucleotide paired-end reads were collected using Illumina version 3 chemistry, and libraries were demultiplexed and assessed for quality and yield using Illumina MiSeq Reporter software.

Sequencing data was analyzed using the MiXCR (version 1.7.2) immune repertoire analysis pipeline (Bolotin et al., 2015). A reference library of strain 129 V_α and V_δ sequences and DBA/J J_α sequences was used for all alignments (Bosc and Lefranc, 2003). Sequences were screened for alignment using the 'align' command with the RNA-seq parameter set (parameter '-p rna-seq'). The 'assemble' command was then used to identify clones from within the pool of aligned sequences, and to assign each clone to a particular V or J segment in a second round of alignment (Table S1). Sequences spanning from the beginning of CDR2 to the end of CDR3 (parameter '-OassemblingFeatures=[CDR2+FR3+CDR3]') were used to identify clones and constituent gene segments (Table S1). Assembled clones were extracted to a human-readable format using the 'exportClones' command and alignment fidelity was assessed manually; frequent mis-identification of *Trav16d* as *Trav16* was corrected by hand. The PlotFancyVJUsage routine in the VDJtools pipeline (Shugay et al., 2015) was used to tabulate clonal frequencies of V-J pairings. Heatmaps were generated using the gplots (Warnes et al., 2016) and RColorBrewer (Neuwirth, 2014) packages within RStudio (R Core Team, 2016), and bar graphs were generated using Excel (Microsoft) and Prism (GraphPad Software, Inc.). For experiments in Figures 1, 3, and 5, subsampling of sequences was performed using the RarefactionPlot routine in VDJtools to verify that the depth of sequencing was sufficient in each sample.

Statistical analysis of repertoire data

Repertoire data from each biological replicate took the form of an 85 × 42 array of counts N_{vj} of the frequency of V_α-J_α combinations at loci V_v and J_j. To estimate the rate of progression along the V_α array relative to progression along the J_α array, for every J_α segment J_j we calculated the frequency weighted average $\overline{V}_J = N_J^{-1}\sum_{i=1}^{85} N_{vj} d_v$, and the frequency weighted SD s_j (where $s_j^2 = (N_j - 1)^{-1}\sum_{v=1}^{85} N_{vj}(d_v - \overline{V}_j)^2$, $N_j = \sum_{v=1}^{85} N_{vj}$ is the marginal frequency of J_α segment J_j and d_V is the distance in base pairs of V_α segment V_i from the most proximal J_α segment). A smoothed spline was fit to the observed mean and SD plots for each strain. Slopes were calculated for the region from *Traj52* to *Traj37*, because this region was linear in all strains.

To compare rates of progression along the V_α array relative to the J_α array between the mouse strains, a mixed effects linear function of the form

$$\overline{V}_{jsi} = \upsilon_{WT,J56} + \upsilon_{s,J56} + b_{si} + rd_j + r_s d_j + \varepsilon_{jsi} \quad (1)$$

was fit to the observed data for wild-type, HYα, and INT1-2-deficient mice. The observed mean V_α segment $\overline{V}_{jsi}$ for strain s (wild-type, HYα, or INT1-2) and replicate i at a given J_α segment j is given as a function of the expected mean Vα segment $\upsilon_{WT,J56}$ for the wild-type strain at initial J_α segment *Traj56*, the effect $\upsilon_{s,J56}$ of strain s at initial J_α segment *Traj56*, a replication-specific initial random effect b_{si} (assumed to have a zero mean Gaussian distribution with SD σ_b), the rate of progression r along the V_α array in the HYα strain as a

function of the distance d_j (in bp) of the j-th J_α segment from *Traj56*, the differential rate r_s of progression along the V_α array in strain s, and measurement error ε_{jsi} (assumed to have an independent zero mean Gaussian distribution with SD σ_e).

To compare between strains how variability in V_α segment usage changed as a function of the J_α segment used, a mixed effects linear function of the form

$$s_{jsi}=\kappa_{WT,J56}+\kappa_{s,J56}+g_{si}+\lambda d_j+\lambda_s d_j+\eta_{jsi} \quad (2)$$

was fit to the observed data for each strain s. The observed SD s_{jsi} in V_α segment usage at J_α segment j in replicate i is given as a function of the SD value $\kappa_{WT,J56}$ of V_α segments at initial J_α segment *Traj56* in wild-type thymocytes, the effect $\kappa_{s,J56}$ of strain s at *Traj56*, the replicate-specific initial random effect g_{si} (given as a zero mean Gaussian distribution with SD σ_g), the rate of increase λ in SD in HYα thymocytes (given as a function of the distance d_j in bp of the j-th J_α segment from the initial J_α segment *Traj56)* the differential rate of increase in SD in V_α segment usage across the J_α array λ_s in strain s, and the measurement error η_{si} (assumed to have an independent zero mean Gaussian distribution with SD σ_h).

Models (1) and (2) were fit to the data by the method of restricted maximum likelihood (REML) using the nlme package in the R computing platform (Pinheiro et al., 2017; R Core Team, 2016). The marginal distribution of counts of cells by J_α segment N_{jsi} for the s-th variant and i-th replicate was separately normalized by the total number of observed cells for each replicatec $\overline{N}_{si}=\sum_{j=1}^{44}N_{jsi}$. We used a two factor ANOVA to examine the relative contributions of the variant type, J_α segment, and their interaction, to the observed variation in marginal distribution.

Modeling and simulation of V_α-J_α rearrangement

Two distinct models for secondary V_α-J_α rearrangement were fit to the observed HYα repertoire. The random choice model assumed that progression in the J_α array is a continuous sequential movement while progression in the V_α array occurs in discrete unidirectional jumps, with the probability of selecting an unused V_α segment from the array V_{i+1}, V_{i+2},…, V_{85}, given by the formula $1/(85-i)$, where V_1 is the most J_α-proximal V_α segment, V_{85} is the most distal V_α segment, and V_i denotes the position of the last V_α segment used. Three sub-models of J_α progression were considered: i) Use of the J_α array one segment at a time, allowing a total of 42 rearrangements per cell, ii) use of J_α segments selected from a Poisson distribution of mean 5 J_α segments distal to the last segment used, and iii) use of J_α segments selected from a Poisson distribution of mean 10 J_α segments distal to the last segment used.

The linear drift model assumed that for a population of cells, progression through the V_α array E[$V(t)$] occurs at a rate r that is proportional to the rate of progression through the J_α array $J(t)$, described by the equation E[$V(t)$] = $V(0)$ + r ($J(t)$ − $J(0)$), where $V(0)$ and J(0) are the V_α and J_α segments used by the primary rearrangement. It was assumed that movement

in the V_α array occurred in discrete steps s and was subject to some random error. For a particular cell c, $V_c(t_s) = V_c(t_{s-1}) + r\,(J_c(t_s) - J_c(t_{s-1})) + \varepsilon_c(t_s)$, where $V_c(t_s)$ and $J_c(t_s)$ were the V_α and J_α segments used in the current rearrangement and $V_c(t_{s-1})$ and $J_c(t_{s-1})$ were the V_α and J_α segments used in the prior rearrangement. The errors $\varepsilon_c(t)$ were assumed to have a zero mean Gaussian distribution with common standard deviation σ_e and independent increments in time. Propagation of the above progression model implied that the position of the V locus $V_c(t)$ accumulates errors over time, as described by $Vc(t_s) = V_c(t_{s-2}) + r\,(J_c(t_s) - J_c(t_{s-2})) + \varepsilon_c(t_s) + \varepsilon_c(t_{s-1}) = V_c(t_{s-3}) + r\,(J_c(t_s) - J_c(t_{s-3})) + \varepsilon_c(ts) + \varepsilon_c(t_{s-1}) + \varepsilon_c(t_{s-2})$, etc. Therefore, the SD in the position of the array $V_c(t_s)$ increases proportionally to the square root of the number of steps s: $\mathrm{SD}[V_c(t_s)] = \sqrt{s}\sigma_e$. For the simulation, the progression rate r and standard deviation σ_e were set to the corresponding quantities in the observed data.

The V_α progression was simulated using each of the probabilistic models described above, for a population of 1000 cells, yielding a set of 1000 V_α-J_α progression trajectories. Each trajectory was initialized by sampling from the observed distribution of V_α segments rearranged to *Traj56* in HYα thymocytes. The simulated trajectories were tallied to obtain an 85 × 42 array of counts R_{jj}, which gave the expected frequency distribution of V_α-J_α combinations under the model. Frequency-weighted mean $\hat{V}_j$ and SD $s_{\hat{V}_j}$ values for V_α segments were graphed against all positions in the J_α array as described for the observed data. Quality of fit of each model to the observed data was measured using the PV calculation, given by the equation:

$$PV = \frac{\sum_{j=1}^{85}\left(\overline{V}_j - \hat{V}_j\right)^2}{\sum_{j=1}^{85}\left(\overline{V}_j - \overline{\overline{V}}_j\right)^2}, \quad (3)$$

where $\overline{V}_j$ is the observed mean V_α segment partner for a given J_α segment, $\hat{V}_j$ the corresponding model prediction and $\overline{\overline{V}}_j$ the overall mean V_α segment across the entire J_α array. The numerator of (3) is the sum of squared errors between the observed and predicted means. The denominator of (3) is the scaled variance of the observed means. For the models averaging steps of 5 or 10 across the J_α array, the sum was calculated over every fifth or tenth J_α segment, respectively.

3C and 4C-seq

3C libraries were generated from 10^7 cells as described (Chen et al., 2015; Hagege et al., 2007; Shih et al., 2012), by digestion with *Hin*dIII. The E_α viewpoint primer and TaqMan probe (Shih et al., 2012) were used in combination with primers annealing to *Hin*dIII fragments containing *Trav13-2*(5′-CTTACAAGTCACAAGAAATCAGAG-3′), *Trav12-3* and *Trav9-3*(5′-GTGAAGTGGCCATAAACATGTTT-3′), and *Trav15-2* (5′-GAAAGAGTGGGCAGGCTTCAGC-3′). Data were normalized to interactions between the E_α viewpoint and its nearest neighboring *Hin*dIII fragment (Shih et al., 2012) using the ΔCt method.

For 4C, secondary digestion and re-ligation were performed as described (Chen et al., 2015; Stadhouders et al., 2013), with modifications. 3C libraries were digested overnight at 37°C with 200 U of *Bfa*I (New England Biolabs), followed by addition of 200 U of *Bfa*I and digestion for 6 h at 37 °C. The digested libraries were purified by phenol-chloroform extraction, precipitated with 2.5 vol ethanol, and rehydrated in 7 ml 30 mM Tris-HCl, pH 8.0, 10 mM $MgCl_2$, 1 mM DTT and 0.1 mM ATP, after which 200 U of T4 DNA ligase (New England Biolabs) were added for overnight incubation at 16°C. The reactio ns were then supplemented with an additional 200 U T4 DNA ligase, followed by incubation for a minimum of 6 h at 16°C. 4C libraries were then purified by phenol-chloroform extraction, precipitated with 2.5 vol ethanol, and rehydrated in 200 μl of 10mM Tris-HCl, pH 8.0, 0.1 mM EDTA. Each library was then used for two rounds of inverse PCR from each of four viewpoints, with eight individual PCR reactions performed per viewpoint. First-round PCR was conducted with the following primers at 0.2 μM: TEA-F (5′-CCATCTGCCTCGCTGTTCTAG-3′) and TEA-R (5′-CTCATAACAGTAACCCAGCAAGCTT-3′), Eα-F (5′-GGCCCTCTCTGTATCTCAGGGGAA-3′) and Eα-R (5′-AAGACAGACCCTGCGAAGCTT-3′), *Traj57-F* (5′-GATCAACAAGTAAACGTTGAAGCTT-3′) and *Traj57-R* (5′-GTATAGCAGCCGACTCCTAG-3′), *Trav14d-3-F* (5′-CTGTTTGAGGTGACAGTACAAGCT-3′) and *Trav14d-3-R* (5′-GGAAAATCCATGCTTAGAGTCTAG-3′), and *Trav1-F* (5′-GTGGTCAACTGCCCCATGCT-3′) and *Trav1-R* (5′-GATGGTGGGAGGTAAGTTCCA-3′). PCR conditions were as follows: 30 s at 98°C, followed by 20 cycles of 10 s at 98°C, 30 s at 60°C and 2 min at 72°C, with a final extension for 10 min at 72°C PCR products were purified with QiaQuick PCR purification reagents (Qiagen) and UPrep spin columns (Genesee), and were then subjected to second round PCR to add Illumina sequencing adapters to their ends. Second round PCR was conducted with the following primers at 0.2 μM: Adapter 2-TEA-F(5′-CCATCTGCCTCGCTGTT-CTAG-3′) and Adapter 1-TEA-R(5′-CTCATAACAGTAACCCAGCAAGCTT-3′), Adapter 2-Ea-F(5′-GGCCCTCTCTGTATCTCAGGGGAA-3′) and Adapter 1-Eα-R(5′-AGACAGACCCTGCGAAGCTT-3′), Adapter *1-Traj57-F*(5′-GATCAACAAGTAAACGTTGAAGCTT-3′) and Adapter *2-Traj57-R*(5′-GTATAGCAGCCGACTCCTAG-3′), Adapter *1-Trav14d-3-F*(5′-CTGTTTGAGGTGACAGTACAAGCT-3′) and Adapter *2-Trav14d-3-R*(5′-GGAAAATCCATGCTTAGAGTCTAG-3′), and Adapter 1-*Trav1-F*(5′-AACTGCCCCATGCTAAGCCT-3′) and Adapter 2-*Trav1-R*(5′-GATGGTGGGAGGTAAGTTCCA-3′), where Adapter 1 is 5′-AATGATACGGCGACCACCGAACACTCTTTCCCTACACGACGCTCTTCCGATCTNNN N-3′ and Adapter 2 is 5′-CAAGCAGAAGACGGCATACGA-3′. PCR conditions were as follows: 30 s at 98°C, 2 cycles of 10 s at 98°C, 30 s at 60°C and 2 min at 72°C, 8 cycles of 10 s at 98°C, 30 s at 65°C and 2 min at 72°C, and a final extension for 10 min at 72°C. All PCR reactions used Phusion polymerase in Phusion HiFi buffer (New England Biolabs) at a reaction volume of 50 μl. Following second round PCR, the eight reactions for each viewpoint were pooled, and PCR products were purified as described above and assessed by gel electrophoresis. PCR products for each viewpoint were quantified with PicoGreen,

multiplexed by pooling all viewpoints from a given biological specimen in equimolar ratios, and supplemented by the addition of a 1% spike of PhiX control library (Illumina). Before sequencing, the quality of the pooled libraries was assessed using the Bioanalyzer platform (Agilent). Multiplexed libraries were then subjected to 100 nucleotide single-end sequencing by the Duke University Sequencing and Genomic Technologies Shared Resource using the Illumina HiSeq 2500 platform. All primers were obtained from Integrated DNA Technologies and dissolved in nuclease-free water. Primers containing Adapter 1 were purified using high-performance liquid chromatography, while all other primers were purified using standard desalting methods.

Sequencing data were analyzed using a workflow modified from one that has been published (Chen et al., 2015; Stadhouders et al., 2013). To generate a reference genome, the strain 129Sv/J *Tcra-Tcrd* sequence was spliced into the mm9 genome assembly in place of the endogenous *Tcra-Tcrd* sequence, as previously performed for *Igh* sequences (Medvedovic et al., 2013). FASTQ files containing raw 'multiplexed' data had the first four random nucleotides excised using the Fastx toolkit, and were split with viewpoint-specific primer sequences included in second round of PCR. The first 14 bp representing viewpoint sequence were excised with the Fastx toolkit, and the remaining 82 nucleotides of each read were aligned to the hybrid mm9$^{Tcra129Sv/J}$ genome assembly using Bowtie, with allowance for 2 mismatches and unique sequences only (Bowtie parameters -v 2 -m 1 –all –best –strata). Mapped reads were counted, sorted, and formatted using Samtools and were visualized using the UCSC Genome Browser. Data are presented as reads per million mapped sequence reads in the *Tcra-Tcrd* locus.

Three-dimensional DNA fluorescence in situ hybridization

3D DNA-FISH was performed as previously described (Shih and Krangel, 2010). Bacterial artificial chromosome (BAC) clones RP23-304L21 (probe A, distal V), RP24-334B8 (probe B, central V), and bMQ-440L6 (probe C, proximal V) were used to generate DNA probes. BACs were directly labeled with Alexa Fluor 568-5-dUTP (ThermoFisher) using a nick translation kit (Roche), with digoxigenin–11-dUTP using a DIG-nick translation kit (Roche), or with biotin-11-dUTP using a biotin-nick translation kit (Roche).

Cells were fixed and hybridized as described previously (Shih and Krangel, 2010). In brief, cells attached to poly-L-lysine-coated slides (VWR Technologies) were fixed in 4% (vol/vol) paraformaldehyde (Electron Microscopy Sciences) for 10 min, followed by permeabilization with 0.5% (wt/vol) saponin (Sigma-Aldrich) and 0.5% (vol/vol) Triton X-100 (VWR) for 1 hr and incubation with 0.1 N HCl for 10 min. After four cycles of freeze/thaw in 20% (wt/vol) glycerol (VWR) in 1× HBSS, the slides were stored at −80°C. For hybridization, the cells were denatured by incubation at 77.8°C for 3 min in 70% (vol/vol) formamide (VWR) and 2× SSC (0.3 M NaCl, 30 mM $Na_3C_6H_5O_7$, pH 7.0), followed by 1 min in 50% (vol/vol) formamide and 2× SSC. Denatured slides were then hybridized for 24–48 h at 37°C with boiled and preannealed probe cocktails. The DNA probe cocktail consisted of 1 μg of each DNA probe per slide and blocking DNAs (mixture of mouse Cot-1 DNA and salmon sperm DNA) in HYBRISOL VII (MP Biomedicals). Excess probe was removed by two incubations of 5–7 min at 42°C in 50% (vol/vol) formamide and 2× SSC,

followed by three incubations at 60°C in 0.2× SSC. The slides were blocked by incubation for 30 min in 4% BSA and 2× SSC and then incubated for 1 h with Cy5-conjugated anti-digoxigenin and AlexaFluor488-conjugated anti-biotin antibodies (Jackson ImmunoResearch Laboratories, Inc.) in 4% (wt/vol) bovine serum albumin and 2× SSC. Excess antibodies were removed by three 5-min incubations in 0.1% (vol/vol) Triton X-100 and 2× SSC. The slides were mounted in Vectashield (Vector Laboratories), and were imaged on an inverted confocal microscope (SP5; Leica) using a 100× NA 1.4 objective lens and a 2× optical zoom. FIJI (National Institutes of Health) software was used to process images and to determine the coordinates (x, y, z) of focus centers. A probe C signal was used to identify *Tcra* alleles as WT (positive) or HYα (weak or absent). Distances between pairs of foci (d, in micrometers) were calculated using the formula $d^2 = [(x' - x) \times 0.151]^2 + [(y' - y) \times 0.151]^2 + [(z' - z) \times 0.131]^2$, where 0.151 μm is the size of each pixel and 0.131 μm is the z-plane separation. Only nuclei with distinguishable signals from two alleles were analyzed.

Statistical methods

Data were analyzed by one-way ANOVA, two-way ANOVA, or MannWhitney U test as appropriate, using Graphpad Prism software. P values of less than 0.05 were considered statistically significant. Sample sizes were estimated on the basis of initial experiments and measurements, rather than being predetermined on the basis of expected effect sizes. No data were excluded from analysis. There was no randomization of mice or “blinding” of researchers to experimental groups.

Supplementary Material

Refer to Web version on PubMed Central for supplementary material.

Acknowledgments

We thank N. Martin and L. Martinek of the Duke Cancer Institute Flow Cytometry Facility for help with cell sorting and analysis, N. Devos of the Duke Center for Genomics and Computational Biology for advice on DNA sequencing, the NIH Tetramer Core Facility for MR1 tetramers, A. Byrd for technical support, and G. Kelsoe and D. Dauphars for comments on the manuscript. Supported by the National Institutes of Health (RO1 GM41052 to M.S.K, and RO1 GM059638 and R21 AG045440 to Y.Z.). K.R.C. was partially supported by the Duke Biostatistics Core, which is funded by the National Center for Advancing Translational Science (UL1TR001117).

References

Abarrategui I, Krangel MS. Regulation of T cell receptor *a* gene recombination by transcription. Nat Immunol. 2006; 7:1109–1115. [PubMed: 16936730]

Aude-Garcia C, Gallagher M, Marche PN, Jouvin-Marche E. Preferential ADV-AJ association during recombination in the mouse T-cell receptor alpha/delta locus. Immunogenetics. 2001; 52:224–230. [PubMed: 11220624]

Bolotin DA, Poslavsky S, Mitrophanov I, Shugay M, Mamedov IZ, Putintseva EV, Chudakov DM. MiXCR: software for comprehensive adaptive immunity profiling. Nat Methods. 2015; 12:380–381. [PubMed: 25924071]

Bosc N, Lefranc MP. The mouse (*Mus musculus*) T cell receptor alpha (TRA) and delta (TRD) variable genes. Dev Comp Immunol. 2003; 27:465–497. [PubMed: 12697305]

Le Bourhis L, Martin E, Peguillet I, Guihot A, Froux N, Core M, Levy E, Dusseaux M, Meyssonnier V, Premel V, et al. Antimicrobial activity of mucosal-associated invariant T cells. Nat Immunol. 2010; 11:701–708. [PubMed: 20581831]

Buch T, Rieux-Laucat F, Forster I, Rajewsky K. Failure of HY-Specific Thymocytes to Escape Negative Selection by Receptor Editing. Immunity. 2002; 16:707–718. [PubMed: 12049722]

Carico, Z., Krangel, MS. Advances in Immunology. Academic Press Inc.; 2015. Chromatin Dynamics and the Development of the TCRα and TCRS Repertoires; p. 307-361.

Chen L, Carico Z, Shih HY, Krangel MS. A discrete chromatin loop in the mouse *Tcra-Tcrd* locus shapes the TCRδ and TCRα repertoires. Nat Immunol. 2015; 16:1085–1093. [PubMed: 26258942]

Ciofani M, Zúñiga-Pflücker JC. Determining γδ versus αβ T cell development. Nat Rev Immunol. 2010; 10:657–663. [PubMed: 20725107]

Corbett AJ, Eckle SBG, Birkinshaw RW, Liu L, Patel O, Mahony J, Chen Z, Reantragoon R, Meehan B, Cao H, et al. T-cell activation by transitory neo-antigens derived from distinct microbial pathways. Nature. 2014; 509:361–365. [PubMed: 24695216]

Cui Y, Franciszkiewicz K, Mburu YK, Mondot S, Le Bourhis L, Premel V, Martin E, Kachaner A, Duban L, Ingersoll MA, et al. Mucosal-associated invariant T cell-rich congenic mouse strain allows functional evaluation. J Clin Invest. 2015; 125:4171–4185. [PubMed: 26524590]

Genolet R, Stevenson BJ, Farinelli L, Østerås M, Luescher IF. Highly diverse TCRα chain repertoire of pre-immune CD8+ T cells reveals new insights in gene recombination. EMBO J. 2012; 31:4247–4248. [PubMed: 23128857]

Glusman G, Rowen L, Lee I, Boysen C, Roach JC, Smit AFA, Wang K, Koop BF, Hood L. Comparative Genomics of the Human and Mouse T Cell Receptor Loci. Immunity. 2001; 15:337–349. [PubMed: 11567625]

Godfrey DI, Uldrich AP, McCluskey J, Rossjohn J, Moody DB. The burgeoning family of unconventional T cells. Nat Immunol. 2015; 16:1114–1123. [PubMed: 26482978]

Warnes, GR., Bolker, B., Bonebakker, L., Gentleman, R., Huber, W., Liaw, A., Lumley, T., Maechler, M., Magnusson, A., Moeller, S., Schwartz, M. gplots: Various R Programming Tools for Plotting Data. 2016. (available at https://cran.r-project.org/package=gplots)

Guo J, Hawwari A, Li H, Sun Z, Mahanta SK, Littman DR, Krangel MS, He YW. Regulation of the TCRα repertoire by the survival window of CD4+CD8+ thymocytes. Nat Immunol. 2002; 3:469–476. [PubMed: 11967541]

Hagege H, Klous P, Braem C, Splinter E, Dekker J, Cathala G, de Laat W, Forne T. Quantitative analysis of chromosome conformation capture assays (3C-qPCR). Nat Protoc. 2007; 2:1722–1733. [PubMed: 17641637]

Hao B, Krangel MS. Long-Distance Regulation of Fetal VS Gene Segment TRDV4 by the *Tcrd* Enhancer. J Immunol. 2011; 187:2484–2491. [PubMed: 21784972]

Hawwari A, Krangel MS. Regulation of TCR S and *a* repertoires by local and long-distance control of variable gene segment chromatin structure. J Exp Med. 2005; 202:467–472. [PubMed: 16087716]

Hawwari A, Krangel MS. Role for rearranged variable gene segments in directing secondary T cell receptor *a* recombination. Proc Natl Acad Sci. 2007; 104:903–907. [PubMed: 17210914]

Hawwari A, Bock C, Krangel MS. Regulation of T cell receptor *a* gene assembly by a complex hierarchy of germline Ja promoters. Nat Immunol. 2005; 6:481–489. [PubMed: 15806105]

Helmink BA, Sleckman BP. The Response to and Repair of RAG-Mediated DNA Double-Strand Breaks. Annu Rev Immunol. 2012; 30:175–202. [PubMed: 22224778]

Hu J, Zhang Y, Zhao L, Frock RL, Du Z, Meyers RM, Meng F, Schatz DG, Alt FW. Chromosomal Loop Domains Direct the Recombination of Antigen Receptor Genes. Cell. 2015; 163:947–959. [PubMed: 26593423]

Huang CY, Kanagawa O. Ordered and Coordinated Rearrangement of the TCR *a* Locus: Role of Secondary Rearrangement in Thymic Selection. J Immunol. 2001; 166:2597–2601. [PubMed: 11160321]

Jhunjhunwala S, van Zelm MC, Peak M, Murre C. Chromatin Architecture and the Generation of Antigen Receptor Diversity. Cell. 2009; 138:435–448. [PubMed: 19665968]

Ji Y, Resch W, Corbett E, Yamane A, Casellas R, Schatz DG. The In Vivo Pattern of Binding of RAG1 and RAG2 to Antigen Receptor Loci. Cell. 2010a; 141:419–431. [PubMed: 20398922]

Ji Y, Little AJ, Banerjee JK, Hao B, Oltz EM, Krangel MS, Schatz DG. Promoters, enhancers, and transcription target RAG1 binding during V(D)J recombination. J Exp Med. 2010b; 207:2809–2816. [PubMed: 21115692]

Kozich JJ, Westcott SL, Baxter NT, Highlander SK, Schloss PD. Development of a dual-index sequencing strategy and curation pipeline for analyzing amplicon sequence data on the MiSeq Illumina sequencing platform. Appl Environ Microbiol. 2013; 79:5112–5120. [PubMed: 23793624]

Livak F, Petrie HT, Crisps IN, Schatz DG. In-frame TCR 8 gene rearrangements play a critical role in the ap/yS T cell lineage decision. Immunity. 1995; 2:617–627. [PubMed: 7796295]

Medvedovic J, Ebert A, Tagoh H, Tamir IM, Schwickert TA, Novatchkova M, Sun Q, Huis in 't Veld PJ, Guo C, Yoon HS. Flexible Long-Range Loops in the VH Gene Region of the *Igh* Locus Facilitate the Generation of a Diverse Antibody Repertoire. Immunity. 2013; 39:229–244. [PubMed: 23973221]

Meierovics A, Yankelevich WJC, Cowley SC. MAIT cells are critical for optimal mucosal immune responses during in vivo pulmonary bacterial infection. Proc Natl Acad Sci. 2013; 110:E3119–E3128. [PubMed: 23898209]

Nakajima PB, Menetski JP, Roth DB, Gellert M, Bosma MJ. V-D-J rearrangements at the T cell receptor S locus in mouse thymocytes of the αβ lineage. Immunity. 1995; 3:609–621. [PubMed: 7584151]

Neuwirth, E. RColorBrewer: ColorBrewer Palettes. 2014. (available at https://cran.r-project.org/package=RColorBrewer)

Parra ZE, Ohta Y, Criscitiello MF, Flajnik MF, Miller RD. The dynamic TCRδ: TCRδ chains in the amphibian *Xenopus tropicalis* utilize antibody-like V genes. Eur J Immunol. 2010; 40:2319–2329. [PubMed: 20486124]

Pasqual N, Gallagher M, Aude-Garcia C, Loiodice M, Thuderoz F, Demongeot J, Ceredig R, Marche PN, Jouvin-Marche E. Quantitative and Qualitative Changes in V-J α Rearrangements During Mouse Thymocytes Differentiation: Implication For a Limited T Cell Receptor a Chain Repertoire. J Exp Med. 2002; 196:1163–1174. [PubMed: 12417627]

Petrie HT, Livak F, Burtrum D, Mazel S. T cell receptor gene recombination patterns and mechanisms: cell death, rescue, and T cell production. J Exp Med. 1995; 182:121–127. [PubMed: 7790812]

Pinheiro, J., Bates, D., DebRoy, S., Sarkar, D., R Core Team. nlme: Linear and Nonlinear Mixed Effects Models. 2017. (available at https://cran.r-project.org/package=nlme)

Pinto FL, Lindblad P. A guide for in-house design of template-switch-based 5′ rapid amplification of cDNA ends systems. Anal Biochem. 2010; 397:227–232. [PubMed: 19837043]

Quigley MF, Almeida JR, Price DA, Douek DC. Unbiased molecular analysis of T cell receptor expression using template-switch anchored RT-PCR. Curr Protoc Immunol. 2011 Chapter 10, Unit10.33.

R Core Team. R: A language and environment for statistical computing. 2016. (available at https://www.r-project.org/)

Schatz DG, Ji Y. Recombination centres and the orchestration of V(D)J recombination. Nat Rev Immunol. 2011; 11:251–263. [PubMed: 21394103]

Schatz DG, Swanson PC. V(D)J Recombination: Mechanisms of Initiation. Annu Rev Genet. 2011; 45:167–202. [PubMed: 21854230]

Shih HY, Krangel MS. Distinct contracted conformations of the *Tcra/Tcrd* locus during *Tcra* and *Tcrd* recombination. J Exp Med. 2010; 207:1835–1841. [PubMed: 20696701]

Shih HY, Krangel MS. Chromatin Architecture, CCCTC-Binding Factor, and V(D)J Recombination: Managing Long-Distance Relationships at Antigen Receptor Loci. J Immunol. 2013; 190:4915–4921. [PubMed: 23645930]

Shih HY, Verma-Gaur J, Torkamani A, Feeney AJ, Galjart N, Krangel MS. *Tcra* gene recombination is supported by a *Tcra* enhancer- and CTCF-dependent chromatin hub. Proc Natl Acad Sci. 2012; 109:E3493–E3502. [PubMed: 23169622]

Shinkai Y. RAG-2-deficient mice lack mature lymphocytes owing to inability to initiate V(D)J rearrangement. Cell. 1992; 68:855–867. [PubMed: 1547487]

Shugay M, Bagaev DV, Turchaninova MA, Bolotin DA, Britanova OV, Putintseva EV, Pogorelyy MV, Nazarov VI, Zvyagin IV, Kirgizova VI, et al. VDJtools: Unifying Post-analysis of T Cell Receptor Repertoires. PLOS Comput Biol. 2015; 11:e1004503. [PubMed: 26606115]

Stadhouders R, Kolovos P, Brouwer R, Zuin J, van den Heuvel A, Kockx C, Palstra RJ, Wendt KS, Grosveld F, van Ijcken W, et al. Multiplexed chromosome conformation capture sequencing for rapid genome-scale high-resolution detection of long-range chromatin interactions. Nat Protoc. 2013; 8:509–524. [PubMed: 23411633]

Thompson SD, Pelkonen J, Hurwitz JL. First T cell receptor alpha gene rearrangements during T cell ontogeny skew to the 5′ region of the J alpha locus. J Immunol. 1990; 145:2347–2352. [PubMed: 2168921]

Tilloy F, Treiner E, Park SH, Garcia C, Lemonnier F, de la Salle H, Bendelac A, Bonneville M, Lantz O. An Invariant T Cell Receptor *a* Chain Defines a Novel TAP-independent Major Histocompatibility Complex Class Ib-restricted a/p T Cell Subpopulation in Mammals. J Exp Med. 1999; 189:1907–1921. [PubMed: 10377186]

Villey I, Caillol D, Selz F, Ferrier P, de Villartay JP. Defect in Rearrangement of the Most 5′ TCR–Jα Following Targeted Deletion of T Early α (TEA): Implications for TCR α Locus Accessibility. Immunity. 1996; 5:331–342. [PubMed: 8885866]

Villey I, Quartier P, Selz F, de Villartay JP. Germ-line transcription and methylation status of the TCR-Jα locus in its accessible configuration. Eur J Immunol. 1997; 27:1619–1625. [PubMed: 9247569]

Weber-Arden J, Wilbert OM, Kabelitz D, Arden B. Vδ Repertoire During Thymic Ontogeny Suggests Three Novel Waves of γδ TCR Expression. J Immunol. 2000; 164:1002–1012. [PubMed: 10623850]

Yu YRA, O'Koren EG, Hotten DF, Kan MJ, Kopin D, Nelson ER, Que L, Gunn MD. A Protocol for the Comprehensive Flow Cytometric Analysis of Immune Cells in Normal and Inflamed Murine Non-Lymphoid Tissues. PLoS One. 2016; 11:e0150606. [PubMed: 26938654]

Zhang B, Wu J, Jiao Y, Bock C, Dai M, Chen B, Chao N, Zhang W, Zhuang Y. Differential Requirements of TCR Signaling in Homeostatic Maintenance and Function of Dendritic Epidermal T Cells. J Immunol. 2015; 195:4282–4291. [PubMed: 26408667]

Zhao L, Frock RL, Du Z, Hu J, Chen L, Krangel MS, Alt FW. Orientation-specific RAG activity in chromosomal loop domains contributes to *Tcrd* V(D)J recombination during T cell development. J Exp Med. 2016; 213:1921–1936. [PubMed: 27526713]

Highlights

- The *Tcra* repertoire is limited by processive V_α−J_α usage on individual alleles
- Processive V_α usage is dictated by an extended *Tcra-Tcrd* chromatin conformation
- V_α diversity during primary rearrangement is imparted by prior *Tcrd* recombination
- *Tcrd* recombination facilitates development of *Trav1-Traj33*$^{+}$ innate-like MAIT cells

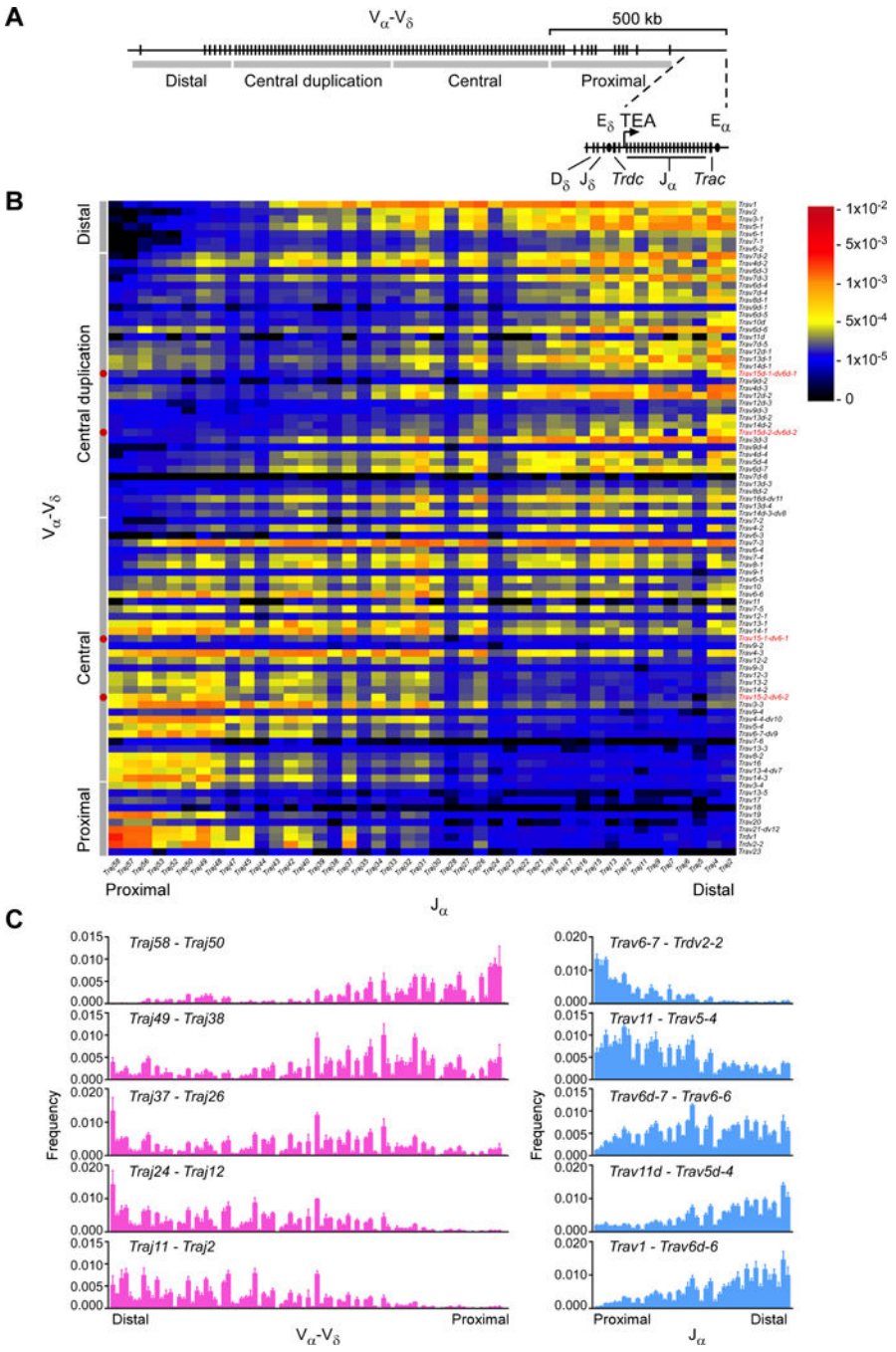

Figure 1. Pre-selection *Tcra* repertoire in strain 129 DP thymocytes

(A) Schematic of the *Tcra-Tcrd* locus, with gene segments, V_α-V_δ array subregions, and c/s-regulatory elements depicted. (B) Frequencies of V_α−J_α rearrangements in strain 129 $CD4^+CD8^+CD3e^{lo}$ thymocytes, as determined by HTS of *Tcra* transcripts amplified by 5′ RACE. V_α-V_δ array subregions are specified along the left border of the plot. Red dots (left border) and red text (right border) identify locations of *Trav15-dv6* family members. (C) Frequencies of V_α-V_δ (left) or J_α (right) usage with the indicated sets of J_α and V_α

segments, respectively. Data are presented as the mean (B) and mean and s.d. (C) of three mice from two independent experiments. See also Table S1.

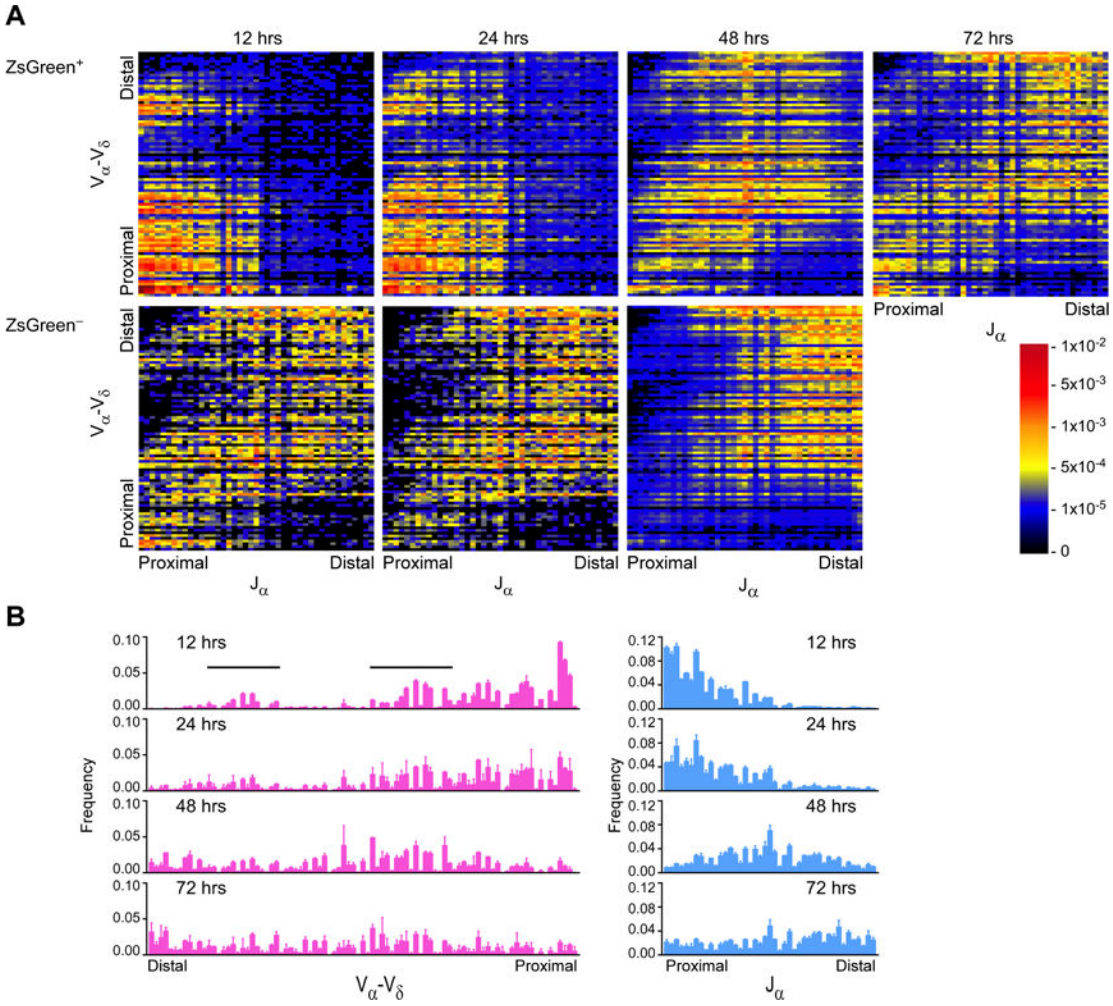

Figure 2. Temporal progression of V_α-J_α rearrangements in strain 129 DP thymocytes

(A) V_α-J_α rearrangement frequencies in $CD4^+CD8^+CD3\varepsilon^{lo}ZsGreen^+$ and $CD4^+CD8^+CD3\varepsilon^{lo}ZsGreen^-$ DP thymocytes sorted from *Tcrd*^{CreER} × *Rosa26*$^{fl\text{-}STOP\text{-}Fl\text{-}ZsGreen}$ mice at the indicated times postinjection of tamoxifen. Lines in the V_α-V_α plot at 12 hrs identify homologous sets of central and central duplication V segments which are targeted for early rearrangement. (B) Frequencies of V_α-V_δ (left) or J_α (right) usage at the indicated time points post-injection. Data are presented as the mean (A) and mean and s.d. (B) of two mice analyzed in two independent experiments, with the exception of the 12- and 24-hr $ZsGreen^-$ analyses, which were conducted once. See also Figure S1.

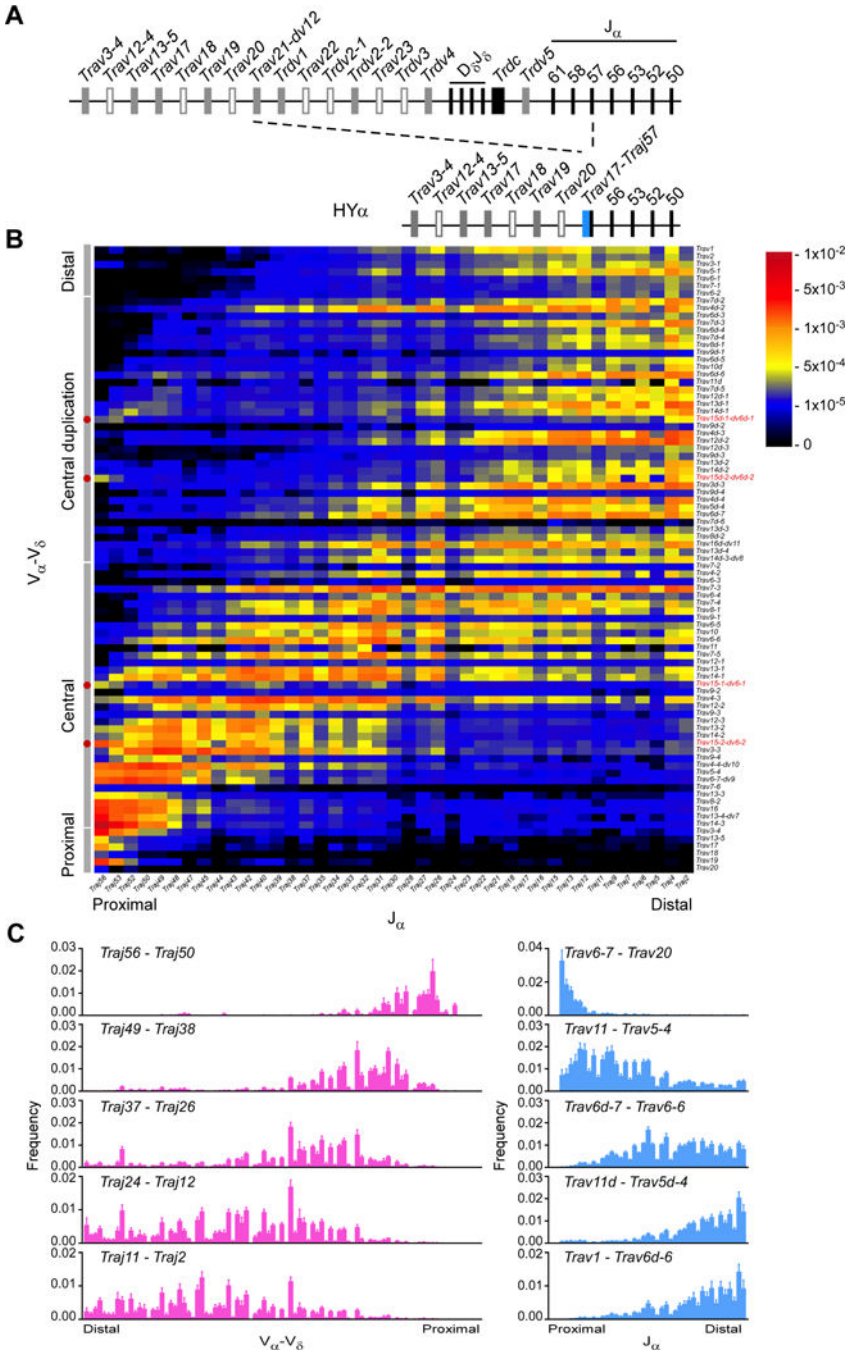

Figure 3. Constrained *Tcra* repertoire in HYα DP thymocytes

(A) Schematic of the HYα *Tcra-Tcrd* locus, depicting insertion of *theTrav17-Traj57* cassette with deletion of 280 kb. (B) Frequencies of V_α-J_α rearrangements in HYα $CD4^+CD8^+CD3\varepsilon^{lo}$ thymocytes. (C) Frequencies of V_α-V_δ (left) or J_α (right) usage with the indicated sets of J_α and V_α segments, respectively. Data are presented as the mean (B) and mean and s.d. (C) of four mice analyzed in two independent experiments. See also Figure S2.

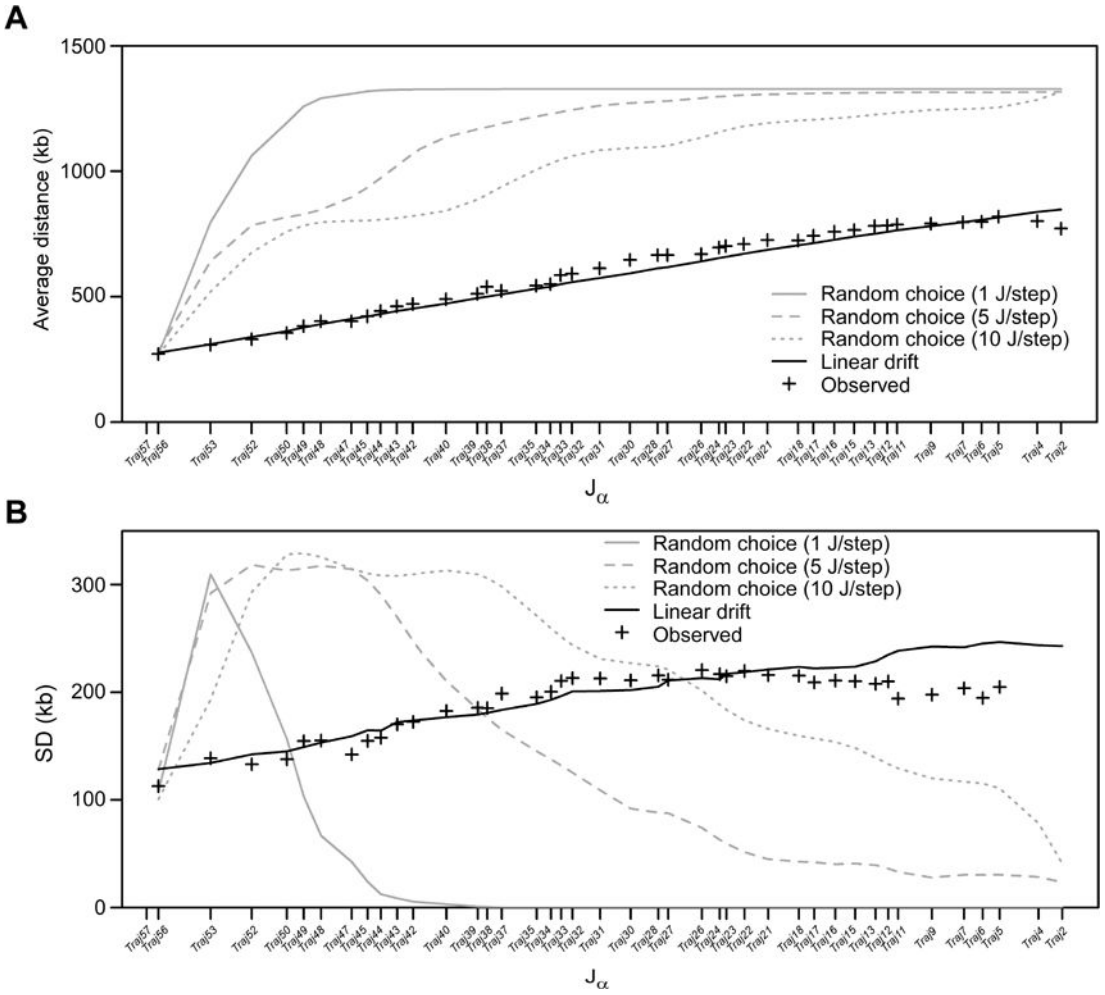

Figure 4. Modeling of V_α-J_α rearrangement in HYα thymocytes

(A) V_α-J_α rearrangements were simulated in 1000 cells assuming either random choice or linear drift models for V segment selection. Results are compared to observed data for HYα thymocytes (Figure 3B), expressed as the frequency-weighted mean of the chromosomal coordinates of the V_α segments used with each J_α segment, with V_α chromosomal coordinates expressed as distance (in kb) from *Traj58*, and J_α segments plotted according to their chromosomal coordinates. PV scores were used to assess fit of each model to observed data. Linear drift, PV=0.06, 0.05 and 0.05, for the 1 J/step, 5 J/step, and 10 J/step simulations of movement along the J_α array, respectively. Only 1 J/step is plotted; 5 J/step, and 10 J/step simulations were superimposable. Random choice, PV=18.55, 12.66, or 6.98 for the 1 J/step, 5 J/step, and 10 J/step simulations, respectively. (B) Frequency-weighted standard deviations of V_α segment usage (in kb) were plotted as a function of J_α segment for the same simulations as in (A), and were compared to the observed data (Figure 3B). See also Table S2.

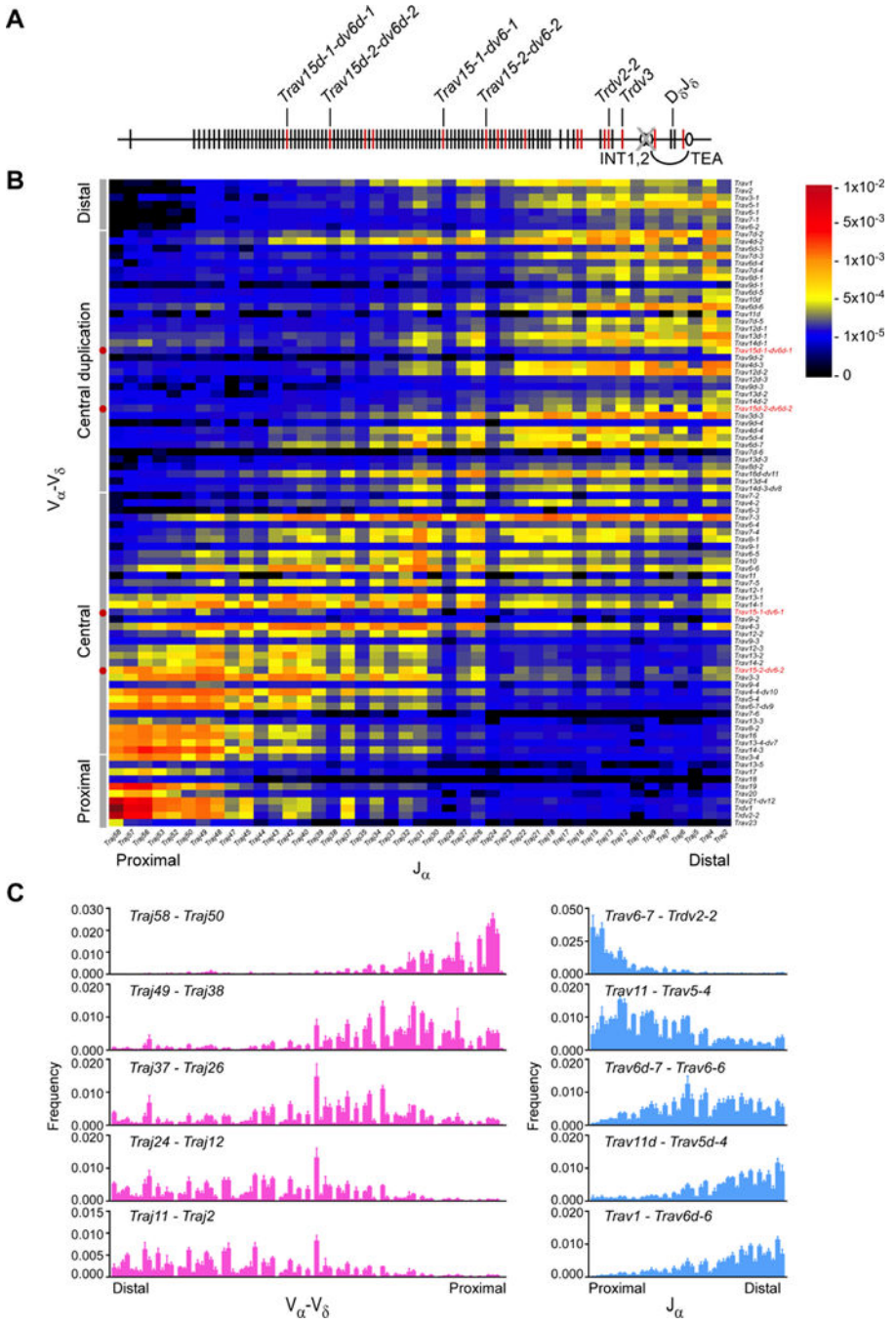

Figure 5. Reduced *Tcra* combinatorial diversity in INT1-2-deficient DP thymocytes

(A) Schematic of the INT1-2-deficient *Tcra* locus, which lacks the INT1 and INT2 CTCF sites and cannot form a chromatin structural loop from INT2 to the TEA CTCF site. V_δ segments are highlighted in red. (B) Frequencies of V_α-J_α rearrangements in INT1-2-deficient $CD4^+CD8^+CD3\varepsilon^{lo}$ thymocytes. (C) Frequencies of V_α-V_δ (left) or J_α (right) usage with the indicated sets of J_α and V_α segments, respectively. Data are presented as the mean (B) and mean and s.d. (C) of three mice analyzed in two independent experiments. See also Figures S3 and S4.

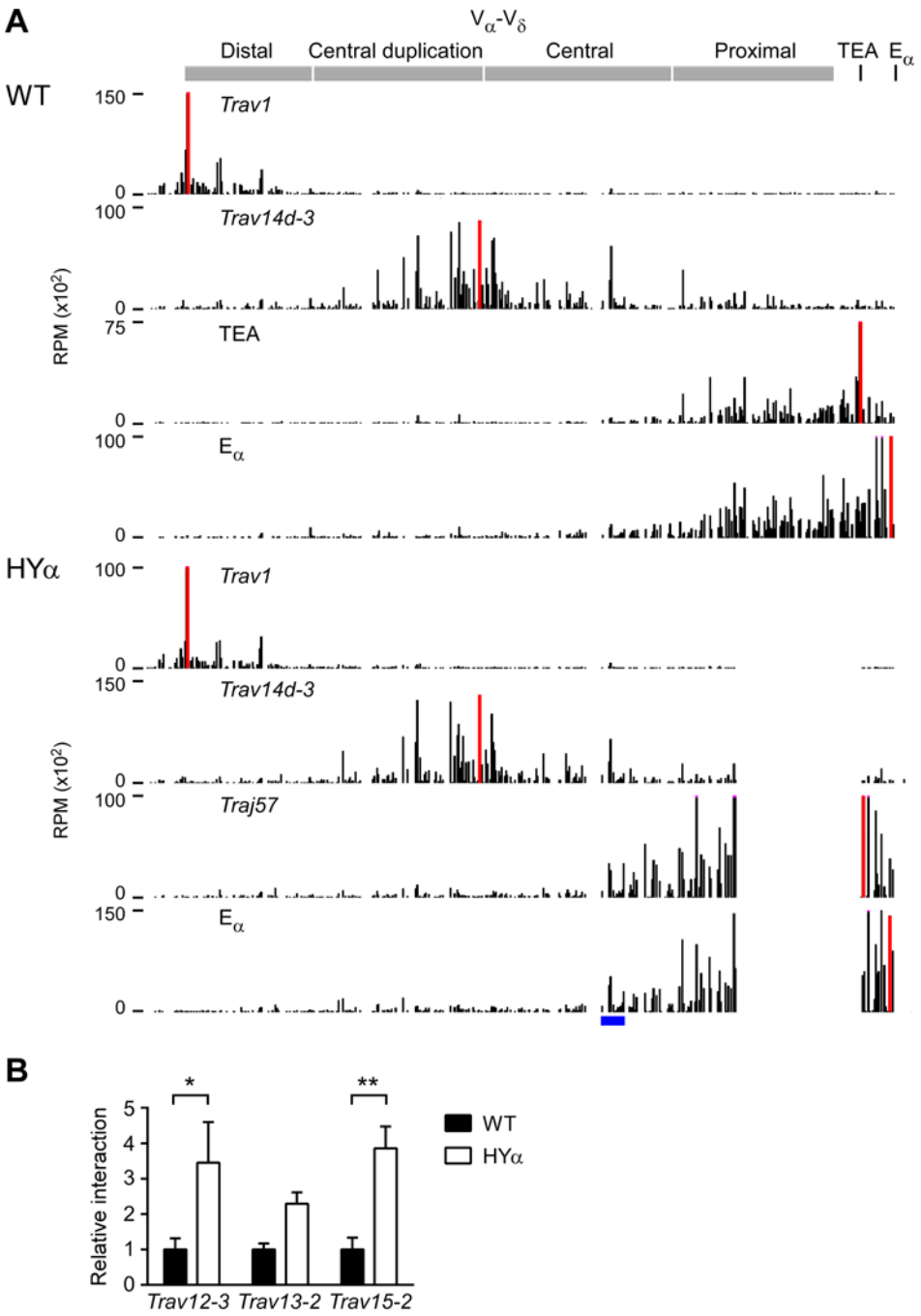

Figure 6. Long-distance DNA contacts on unrearranged and HYα alleles

(A) 4C-seq profiles of interactions with the specified viewpoints on wild-type (top) and HYα (bottom) *Tcra* alleles in DP thymocytes generated in *Rag2*$^{-/-}$ mice and HYα *Rag2*$^{-/-}$mice, respectively. Data are presented as reads per million mapped reads (RPM) within the *Tcra-Tcrd* locus. In each panel, the red bar identifies the viewpoint fragment. The gaps in the HYα profiles reflect the 280 kb deletion on this allele. Data are representative of two independent experiments. The blue bar beneath the HYα plots marks the region containing V segments analyzed by 3C. (B) 3C measuring interactions between E_α and

selected central V_α segments. Data for WT and HYα were first normalized to each other based on interaction between E_α and a nearest neighbor fragment, and results for HYα at each site were then expressed relative to those for WT. Data are presented as the mean and s.e.m. of 5–6 WT and 3–4 HYα mice analyzed in two independent experiments. $*P < 0.001$, $**P < 0.0001$, by two-way ANOVA with Sidak's multiple comparisons test. See also Figure S5.

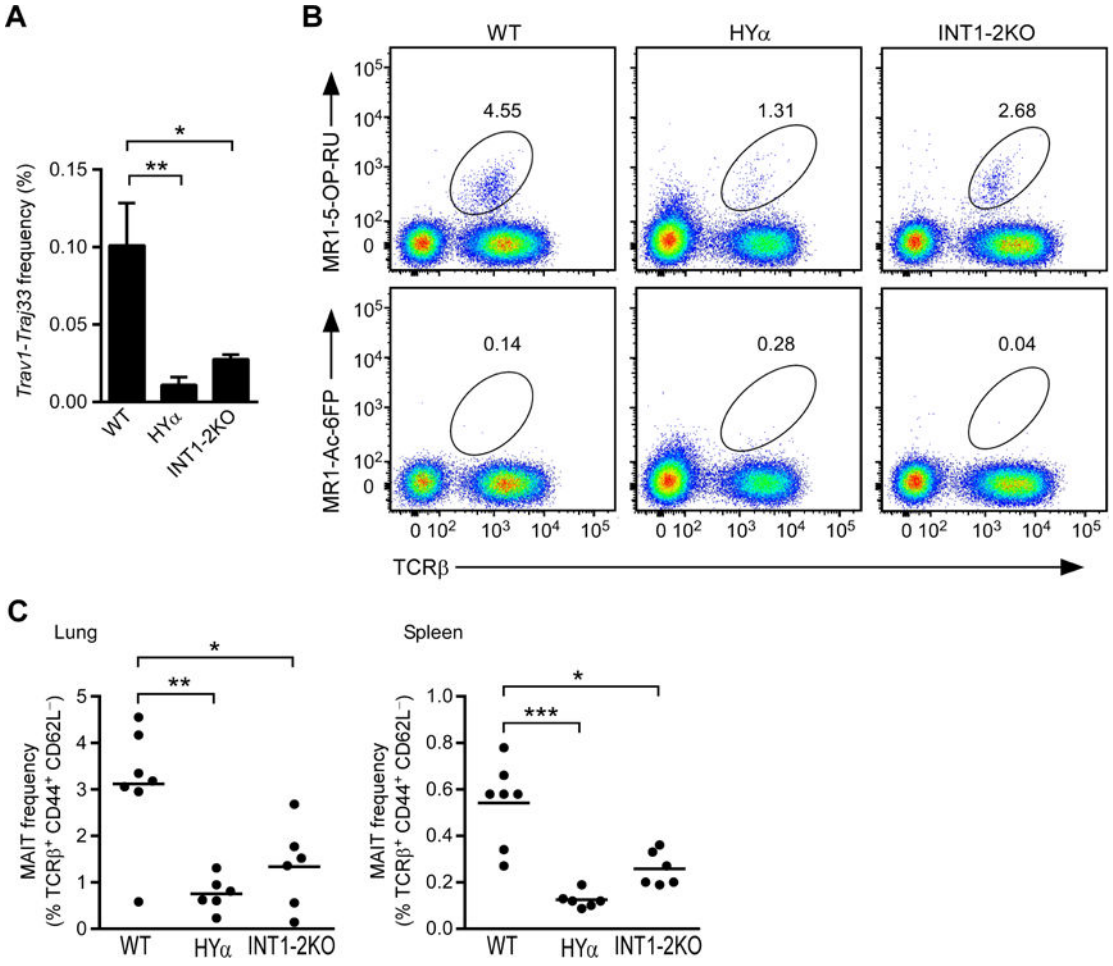

Figure 7. Diminished MAIT cell frequencies in HYα and INT1-2-deficient mice

(A) Frequency of *Trav1-Traj33* rearrangement in wild-type, HYα, and INT1-2-deficient thymocytes as determined by HTS. Data represent the mean and s.d. of 3–4 mice for each genotype. (B) Representative flow cytometry of lung cells isolated from wild-type, HYα, and INT1-2-deficient mice, stained for TCRβ and MR1-tetramers loaded with the indicated antigens. Numbers indicate the percentage MR1-tetramer positive cells within $TCR\beta^+$ population, with pre-gating for $7AAD^-Lin^-CD62L^-CD44^+$. (C) Quantification of MAIT cell frequencies in lungs (left) and spleens (right) of wild-type, HYα, and INT1-2-deficient mice. Horizontal lines indicate the mean for each genotype, with 6–7 mice analyzed in 5 independent experiments. $*P < 0.01$, $**P < 0.001$, and $***P<0.0001$, by one-way ANOVA, with Dunnett's multiple comparisons test.